Numerical investigation of upstream cylinder flow and characterization of forming fabrics

Papermaking

Gustav Kettil*, Andreas Mark, Kenneth Wester, Mats Fredlund and Fredrik Edelvik

Numerical investigation of upstream cylinder flow and characterization of forming fabrics

https://doi.org/10.1515/npprj-2018-0072
Received November 6, 2018; accepted June 17, 2019; previously published online July 12, 2019

Abstract: In this work, the fundamentals of upstream flow over cylinders and forming fabrics are investigated, and measures for characterization of fabrics are proposed. Two-dimensional flow over one cylinder, two cylinders, and one and two rows of cylinders, are analysed numerically. By studying different configurations and various Reynolds numbers, the upstream flow features are characterized. It is concluded that cylinders have a short range of upstream flow impact, shortest for rows of cylinders with small spacings. For $Re \in [10, 80]$, the Reynolds number dependency is weak. It is shown that a downstream row positioned in tandem has negligible impact on the upstream flow, while a displaced second row influences the upstream flow if the spacing in the first row is larger than one diameter. The pressure drop required to drive the flow over the cylinders depends non-linearly on the porosity of the configuration. Flow measures of the upstream flow are proposed, which in addition to the volume flow per area are used to characterize fabric flow properties. The conclusions from the cylinder study also hold for industrial fabrics, and it can be explained how properties of the fabric influence the final paper. The wave-length of flow periodicity is studied in relation to drainage marking. This study demonstrates that simulations can greatly improve pure experimental-based fabric characterization.

Keywords: drainage marking; flow uniformity; forming fabrics; forming fabric parameters; upstream cylinder flow.

***Corresponding author: Gustav Kettil,** Fraunhofer-Chalmers Centre, Chalmers Science Park, SE-412 88 Gothenburg, Sweden; and Chalmers University of Technology and University of Gothenburg, Mathematical Sciences, SE-412 96 Gothenburg, Sweden, e-mail: gustav.kettil@fcc.chalmers.se
Andreas Mark, Fredrik Edelvik, Fraunhofer-Chalmers Centre, Chalmers Science Park, SE-412 88 Gothenburg, Sweden, e-mails: andreas.mark@fcc.chalmers.se, fredrik.edelvik@fcc.chalmers.se
Kenneth Wester, Albany International, Box 510, SE-301 80 Halmstad, Sweden, e-mail: kenneth.wester@albint.com
Mats Fredlund, Stora Enso, Research Centre Karlstad, SE-650 09 Karlstad, Sweden, e-mail: mats.fredlund@storaenso.com

Introduction

In the forming section of a paper machine, the basic structure of paper is formed. The formation ensues when pulp fibers, diluted in water, are released from the head-box and flow down onto the forming fabric. Finally, the fibers lay down on the fabric and the paper structure is built up while much of the water passes through the openings of the fabric at speeds about 0.05–0.5 m/s (Green et al. 2008). The formation is a complex process, governed by the fabric structure, the rheology of the suspension, and the accumulation of fibers. During the dewatering, the flow is initially dominated by the fabric structure. When fibers accumulate, the flow field changes, re-directing incoming fibers to areas with higher flow rate.

It is desirable to control the mechanical properties of paper products, and one way would be by controlling the flow conditions during forming, with an aim of reaching a desired paper structure. Both the mass distribution and the fiber orientation are affected by the fabric structure (Danby 1986, Helle 1978), and both obviously impact the paper properties. Increasing the understanding of how the fabric geometry influences the flow, and in turn the lay down process, is an important step towards a more extensive control of the paper forming process. If fabrics can be tailored to fulfil certain demands on the resulting paper, such as uniform density, or a specific orientation of fibers, product development would be significantly enhanced.

A wide variety of forming fabrics are used in different paper machines, depending on which type of paper product that is produced. To be able to classify properties of different fabrics, and their influence on the properties of the end-product, it is necessary to have measures which capture the characteristics well enough. One measure is the CFM-value, defined as the volume flow of air per area through a fabric for a certain applied pressure drop, measured in feet per minute. However, this measure alone does not describe the fabric properties well enough (Kortelainen et al. 2008). Therefore, other measures, describing a wider range of characteristics of fabrics, are needed. Moreover, due to lack of measuring methods (Kortelainen et al. 2008), experimental investigations of fabrics are dif-

ficult, making simulation tools important for further analysis. Frameworks for simulation of fiber lay down, for example the works of Mark et al. 2011a, Svenning et al. 2012, and Kettil 2016, also benefit from a more throughout understanding of fabric flow characteristics.

Forming fabrics are woven materials with complex structure. However, their basic building blocks, threads with different diameters, have a simple geometry. By studying simplified structures, built up of cylinders, fundamental understanding can be attained, necessary to later understand the features of the complex flow over industrial fabrics. Investigation of different two-dimensional configurations of cylinders, each cylinder representing a fabric thread, is a first step towards such a fundamental understanding of how flows over fabrics behave, and influence the paper forming process.

Flow over one cylinder has been a research topic for a long time, and profound development, such as the first studies of vortex streets (Benard 1908, Von Karman and Rubach 1912) were elaborated already over hundred years ago. Zdravkovich (1997) states that the Reynolds number is the governing parameter for disturbance-free two-dimensional flow over one cylinder. Moreover, the flow features can be divided into main categories based on whether the flow is steady and symmetric, steady and asymmetric, unsteady and laminar, or unsteady and turbulent. Roshko's (1954) experiments show that transition from steady to unsteady flow occurs around $Re = 40$, and that turbulence arises around $Re = 150$. The transition from symmetric to asymmetric flow occurs around $Re = 5$ (Zdravkovich 1997).

Studies of the flow over two cylinders also have a long history. Due to infinitely many possible different configurations of two parallel cylinders, two main cases, tandem and side-by-side with uniform diameters, have attained most attention. In addition to the Reynolds number, which is the main parameter when investigating flow over one cylinder, the spacing is an additional main parameter when studying two cylinders. Zdravkovich (1977) has reviewed different studies of two-cylinder flow, and the majority focuses on high Reynolds number regimes and primarily on the downstream features.

Flows over more than two cylinders or rows of cylinders have not been studied as extensively as flows over one and two cylinders. The existing studies mostly cover high Reynolds numbers and focus on the downstream wake behaviour.

Relatively few studies of flow over forming fabrics exist in the literature. Huang et al. (2006) simplified the fabric structure and simulated the flow over one and two cylinder rows for Reynolds numbers from 30 to 100. They analysed the wake behaviour for some different displacements between the cylinders. Some preliminary results regarding the upstream features were presented, concluding that if the row spacing is larger than one diameter, the upstream effects from the second row are negligible.

Gilchrist and Green (2009) experimentally investigated the flow through a bank of cylinders representing a simplified forming fabric for $Re = 65$. The results indicate that displacing the second row such that its cylinders are below the holes of the first row has an impact on the upstream flow. They concluded, similarly as Huang et al. (2006), that for spacings between the two rows larger than 0.7 diameters, the second row did not affect the upstream flow.

Green et al. (2008) simulated the flow through fabric-like structures with one layer of sinusoidal woven cylinders. They investigated how much the displacement of single filaments affected flow rate through the woven structure and found that the effect is highly localized. Later, Vakil et al. (2009) developed a method to create CAD geometries of real forming fabrics and used these to perform forming fabric flow simulations. The simulations showed that the maximum upstream velocity component perpendicular to the fabric plane could be three times higher than the minimum, stating that up to three times more fibers will accumulate in certain areas during the initial lay down.

The aim of this work is to clarify the upstream features of the flow over one and two rows of cylinders with uniform diameters, by focusing on the dependency on Reynolds number, steady versus unsteady flow, and investigating how different spacings between cylinders in each row, and also between rows, as well as how displacing the second row, affect the upstream flow. Additionally, measures of the upstream flow impact are proposed, to enable comparison of different cylinder structures and how they influence the upstream flow. The purpose of introducing these measures is to be able to apply them to real forming fabrics, enabling comparison of flow characteristics. Furthermore, the observations from the cylinder study, together with the measures of flow impact are applied to three industrial fabrics, demonstrating how different types of fabrics can be compared. Moreover, fabric flow patterns increasing the risk of drainage marking are investigated and the simulations help to clarify its causes.

In the Method section, the numerical flow solver, IBOFlow, is described. In the same section, the different simulation setups are specified, and the validation of the numerical method is shown. Moreover, the three industrial forming fabrics are presented. In the Results and discussion section, the results of the cylinder study are presented

and discussed. Results for the three-dimensional flow over the three industrial fabrics are shown and compared with the cylinder study. In the last section, the conclusions and summary of the main results are stated.

Method

The fluid flow is described by the Navier Stokes equations, and the coupling between object and fluid is treated by an immersed boundary method. The Navier-Stokes equations for an incompressible fluid read

$$\rho \frac{\partial u}{\partial t} + \rho u \cdot \nabla u - \mu \nabla^2 u = -\nabla p, \tag{1}$$

$$\nabla \cdot u = 0, \tag{2}$$

where u is the fluid velocity, p is the pressure, and ρ and μ are the density and dynamic viscosity of the fluid, respectively.

Fluid solver

The flow is solved using IBOFlow® (Immersed Boundary Octree Flow Solver) (Mark et al. 2011b), which is an in-house multi-phase flow solver for incompressible fluids. The equations, Equations (1)–(2), are discretized using the finite volume method and solved separately. The SIMPLEC method, developed by van Doormaal and Raithby (1984), is used to couple the segregated pressure and velocity fields. A Cartesian octree grid is used, enabling efficient dynamical refinements. The solution variables are co-located, and to suppress pressure oscillations the Rhie-Chow interpolation (Rhie and Chow 1983) is adopted.

The mirroring immersed boundary method developed by Mark and van Wachem (2008), and extended by Mark et al. (2011b), constrains the velocity at the boundary surface of the immersed object by an implicit condition attained by mirroring or extrapolating the prescribed surface velocity to nearby fluid cells. The fictitious velocity field arsing at the inside of the immersed boundary is excluded from the continuity equation ensuring zero mass flow over the surface.

Simulation setups

Four main cases of two-dimensional cylinder flow are investigated: the flow over one and two cylinders, and the flow over one and two rows of cylinders. Two different types of domains are used, one type for the flow over one and two cylinders, and one type for the row configurations. In both types, the cylinders are positioned parallel to the z-axis, leading to a two-dimensional setup in the x-y plane. Since Reynolds numbers $Re \in [10, 80]$ are considered in this work, and turbulence usually occurs for higher Reynolds numbers (Roshko 1954), it is assumed that the two-dimensional simplification holds true. The flow is driven by a fixed inlet velocity at the upper horizontal boundary. See Figure 1 for an illustration of the domain for two cylinders. The x-velocity is denoted u and the y-velocity is denoted v. Note that the v-velocity is defined to be positive in the negative y-direction. The cylinder diameter is denoted d and the surface spacing is denoted S.

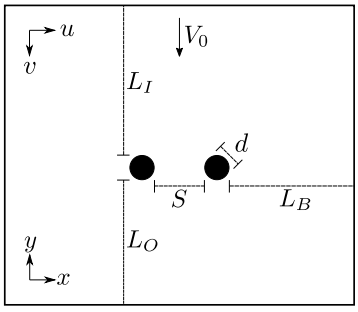

Figure 1: Simulation domain for two cylinders side-by-side.

For the case of two cylinders, two different configurations are studied, tandem and side-by-side, depicted in Figure 2. Likewise, for two rows of cylinders, two types of configurations are examined, tandem and displaced, illustrated in Figure 2. In the displaced configuration, the same displacement is used for all cases, corresponding to a shift of the downstream row equal to half the x-distance between cylinder centers.

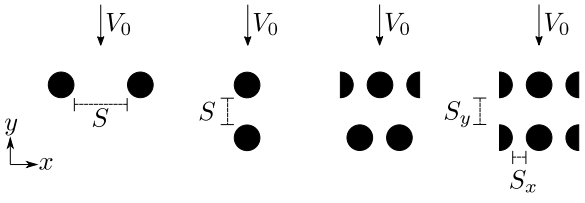

Figure 2: The four main configurations of cylinders: two cylinders side-by-side, two cylinders tandem, two rows displaced, and two rows tandem.

The notation S may denote the surface spacing in both x- or y-direction while the notation S_x and S_y is used to clarify which direction that is regarded. Using these notations,

the normalized surface spacings in horizontal and vertical direction are defined according to

$$g = \frac{S_x}{d}, \qquad l = \frac{S_y}{d}. \tag{3}$$

Next, the size of the rectangular simulation domain is specified. For all cases, the vertical distance from the upper boundary to the uppermost cylinder is $L_I = 70d$. The vertical distance from the lowermost cylinder to the bottom boundary is $L_O = 50d$. For the simulations with one and two cylinders, the horizontal distance from the vertical boundaries to the outermost cylinder is $L_B = 70d$. These are relatively large values compared to other numerical studies, and the blockage effect with this setup is small. See the work of Pozdziech and Grundmann (2007) for a comprehensive study of the domain size for one-cylinder flow. For the simulations with one or two rows of cylinders, the horizontal setup of the domain differs compared to the case of one and two cylinders, as a cyclic boundary condition is utilized, as indicated in Figure 2.

The fluid domain is represented by a quadtree grid, enabling straightforward refinement. For the cylinder simulations, the base cell size is equal to the cylinder diameter. A refinement level corresponds to dividing a squared cell into four equally sized squares. Seven refinement levels are used around the cylinder surfaces ranging seven diameters out from the surface, resulting in $2^7 = 128$ cells over the cylinder diameter. Grid convergence is assured by altering the number of refinements and the distance of refinements away from the cylinder while comparing values of drag, pressure and velocity. For example, the two cases of one row of cylinders with $g = 1$, and two rows of cylinders with $g = 3$, $l = 0.5$ and the second row displaced, are compared. For the v- and u-velocity profiles at $0.25d$ upstream, the relative L^2-differences between the given grid and one with one additional refinement, are less than $3 \cdot 10^{-3}$. For the unsteady cases, the wake is refined five levels ($2^5 = 32$). For further analysis of the grid convergence of the well-validated simulation framework, see (Mark et al. 2011b).

The flow is driven by an inlet velocity at the upper horizontal boundary, where the v-velocity is imposed as $v = V_0$, where V_0 is a constant. At the same boundary, the pressure is prescribed with a Neumann condition. At the lower horizontal boundary, an outlet condition is specified by setting the pressure to zero while the velocity is restrained by a Neumann condition. In the simulations with one or two cylinders, symmetry conditions are imposed at the vertical boundaries, with Neumann conditions for pressure and velocity. For simulations with rows of cylinders, cyclic boundary conditions are used at the vertical boundaries.

Simulations are performed with Reynolds numbers in the range 1–100, with emphasis on 10–80. Around $Re = 40$ the transition from steady to unsteady flow occurs. For the steady flow simulations, a steady state solver is used, while a transient solver is used otherwise.

In addition to the two-dimensional simulations of the flow over cylinders, three-dimensional simulations of the flow over forming fabrics are performed. A rectangular box is used as simulation domain and the fabric is positioned in the x-y-plane, perpendicular to the z-axis. The flow is driven either by a fixed inlet velocity or a pressure drop, resulting in a flow in the negative z-direction. The z-direction is positive out from the paper side of the fabric. As for the cylinder flows, the z-velocity is defined to be positive in the negative z-direction. The x-y dimensions of the domain is equal to the size of the piece of a forming fabric used. At the boundaries surrounding the domain, symmetry boundary conditions are imposed.

In Figure 3, triangulations generated from tomography images of the three different forming fabrics studied in this work are shown. Fabric A is a conventional double layer fabric. Fabric B is a warp bound triple layer fabric. Fabric C is a fine sheet support binder fabric. Fabric A and Fabric C are mainly used on graphical papers (newsprint, LWC- and SC-paper), but also for the printing ply on high quality board (LPB and FBB). Fabric C is newer and has in many cases replaced Fabric A, due to its better retention and wear resistance. Fabric B is mainly used on different packaging applications, as on filler plies on multi-ply board machines and on liner and fluting machines.

Air with density $\rho = 1.2\,\mathrm{kg/m^3}$, and with viscosity $\mu = 18.1 \cdot 10^{-6}\,\mathrm{kg/ms}$ is used in the fabric simulations. Air is normally used when measuring the CFM-value of fabrics and when investigating flow properties of fabrics experimentally. In this work, we restrict our simulations of the flow over fabrics to the case of air. The base grid cell size is 0.1 mm with three refinement levels around the fabric surface ranging 0.5 mm out from the surface. The total height of the domain is 6 mm and the distance from the bottom of the fabric to the outlet boundary is 3 mm.

Validation

To demonstrate the accuracy of the numerical method, a validation for flow over one cylinder is presented in Figure 4, where the drag force coefficients from Tritton's experiments (Tritton 1959) for different Reynolds numbers are compared with simulated values. The drag force coefficient is calculated as $C_D = \frac{F}{2\rho V_0^2 d}$, where F is the magnitude of the force acting on the cylinder.

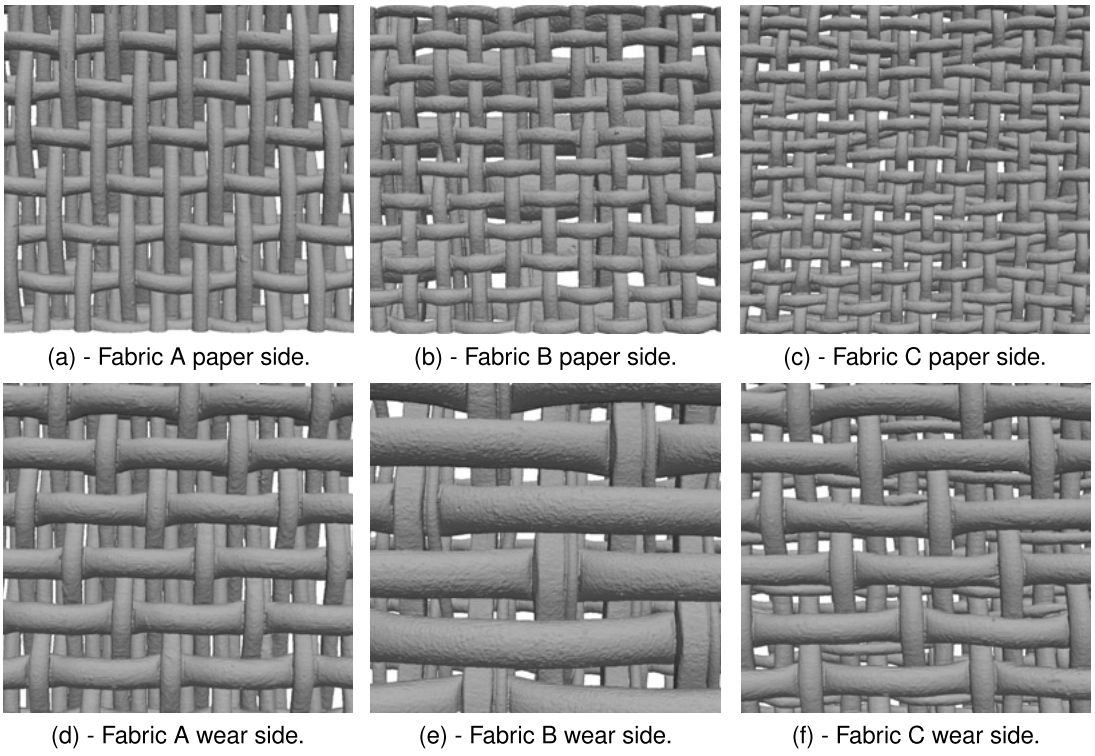

Figure 3: Triangulations of the three forming fabrics studied in this work, generated from tomography images. The snapshots are from above (paper side) and from below (wear side). The dimensions are approximately 3 mm × 2.8 mm ($x \times y$).

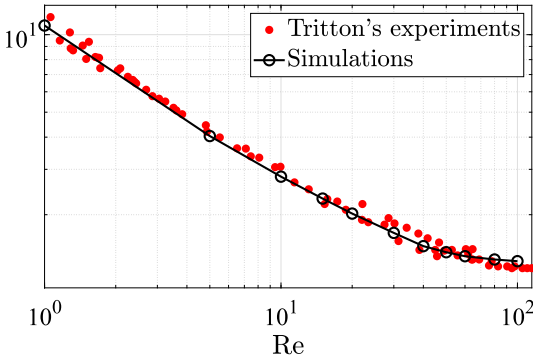

Figure 4: Experimental and simulated values of the drag force coefficient $C_D = \frac{F}{2\rho V_0^2 d}$ for flow over one cylinder.

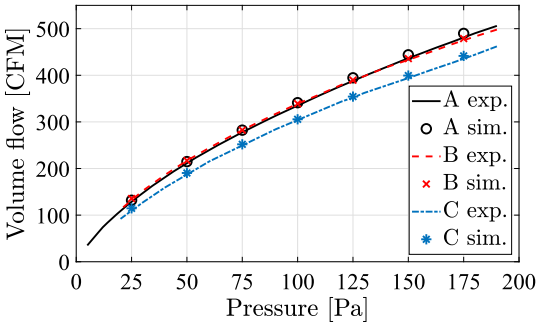

Figure 5: Experimental and simulated values of the volume flow of air per area through the three forming fabrics.

Further, three-dimensional simulations of the air flow over the three forming fabrics are performed and compared with experimental values. In Figure 5, the volume flow of air per area is shown for different applied pressure drops. The volume flow per area is given in the unit CFM, corresponding to feet per minute, which is common when characterising forming fabrics. In the same plot, the corresponding experimental results are shown and it can be seen that the simulations give excellent agreement.

Results and discussion

In this section, the simulation results are presented and discussed. Emphasis is on upstream flow features. First, one cylinder is examined to obtain an understanding of the basics of upstream cylinder flow. Thereafter aspects of two cylinders are presented before the setups with one and two rows of cylinders are analysed in detail. The cylinder results are concluded with an overview using various general measures. Finally, the flow over three industrial

forming fabrics is investigated and compared with the cylinder study.

Flow over one cylinder

In Figure 6, the v-velocity field of the flow over one cylinder is plotted for $Re = 20$. The flow is normalized with the main stream velocity V_0.

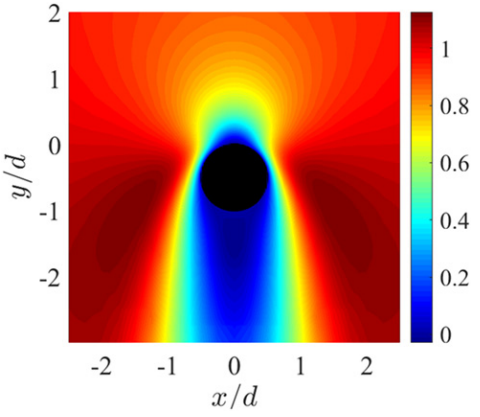

Figure 6: Normalized v/V_0-velocity field for flow over one cylinder at $Re = 20$.

In Figures 7–8, the v- and u-velocity profiles are shown. The profiles are extracted at three different distances upstream, $y/d \in \{0.25, 0.5, 1\}$.

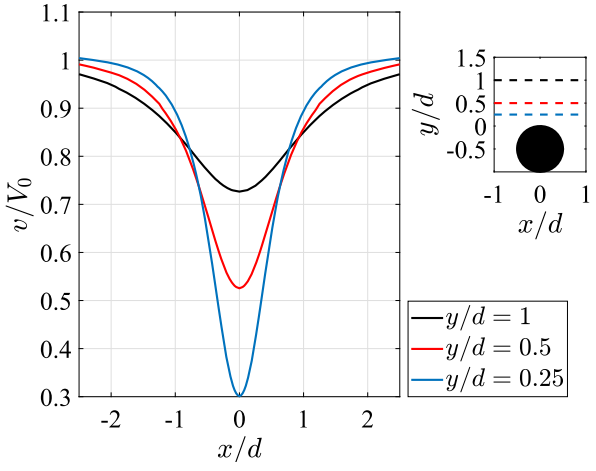

Figure 7: Normalized velocity profiles v/V_0 for flow over one cylinder at $Re = 20$, extracted at three different positions upstream, $y/d = 1$, $y/d = 0.5$ and $y/d = 0.25$.

At each y/d-position vertically upstream, the maximum and minimum value of the velocity profile at that particular position are extracted, resulting in extreme value functions defined as

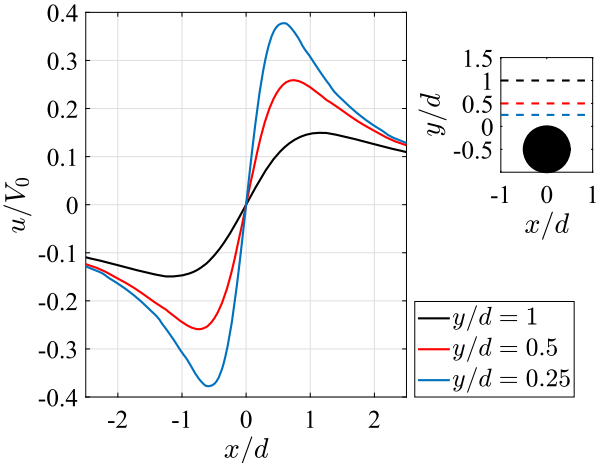

Figure 8: Normalized velocity profiles u/V_0 for flow over one cylinder at $Re = 20$, extracted at three different positions upstream, $y/d = 1$, $y/d = 0.5$ and $y/d = 0.25$.

$$M_v\left(\frac{y}{d}\right) = \max_{x \in W} \frac{v(x,y)}{V_0}, \tag{4}$$

$$m_v\left(\frac{y}{d}\right) = \min_{x \in W} \frac{v(x,y)}{V_0}, \tag{5}$$

$$M_u\left(\frac{y}{d}\right) = \max_{x \in W} \frac{|u(x,y)|}{V_0}, \tag{6}$$

where $W = [-w, w]$ for some large value w. In Figure 9, the extreme value functions for the flow over one cylinder are plotted.

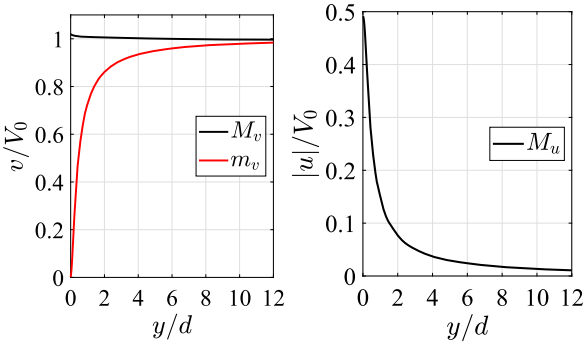

Figure 9: Extreme value functions for v (left) and u (right) for the flow over one cylinder at $Re = 20$.

Level curves for the v- and u-velocities are plotted in Figures 10–11. The level curves are extracted at different percent values of the main stream velocity, enclosing regions where the velocity is influenced more than a

given percent value of the main stream velocity. The region where the reduction of the v-velocity is more than 30 % is only about the same size as the cylinder itself. The region with impact less than 10 % is much larger, almost $3d$ in diameter. This indicates that the impact on the cylinder is large close to the cylinder but decays rapidly away from the surface.

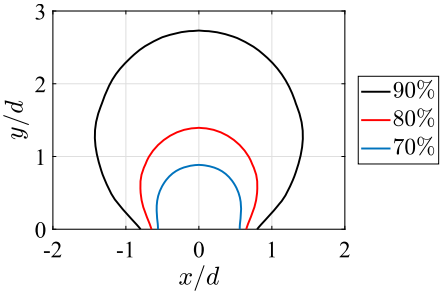

Figure 10: Level curves for v/V_0 at 0.9, 0.8 and 0.7 for the flow over one cylinder at $Re = 20$.

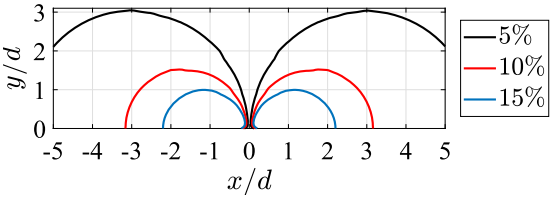

Figure 11: Level curves for $|u|/V_0$ at 0.05, 0.1 and 0.15 for the flow over one cylinder at $Re = 20$.

The preceding results are all for $Re = 20$. The Reynolds number dependency on the upstream flow features is discussed next. In this work, emphasis is on Reynolds numbers in the range 10–80. Around $Re = 40$, the transition from steady to unsteady occurs, leading to an essential change in behaviour of the downstream flow. However, varying the Reynolds number in the range 10–80 has remarkably small impact on the upstream flow characteristics, as will be seen next. In Figures 12–13, the velocity profiles for v and u at $y/d = 0.5$ are shown for $Re \in \{1, 5, 10, 15, 20, 30, 40, 60, 80\}$.

The shapes of the velocity profiles are similar, with an upward translation for increasing Reynolds number. The profile for $Re = 1$ stands out. This case of creeping flow is however outside the scope of interest. Any effect of the transition from steady to unsteady, around $Re = 40$, cannot be seen in the velocity profiles. This indicates that in the Reynolds number range 10–80, it is sufficient to study

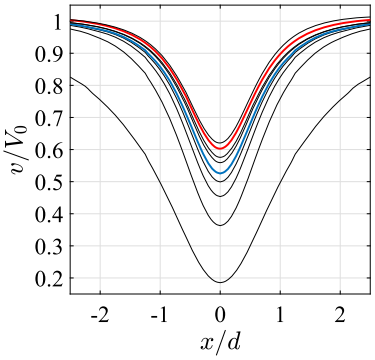

Figure 12: The v/V_0-velocity profiles at $y/d = 0.5$ for $Re \in \{1, 5, 10, 15, 20, 30, 40, 60, 80\}$ for the flow over one cylinder. The lowest curve is for $Re = 1$ and each increment in Reynolds number corresponds to moving up one curve in the plot. The case of $Re = 20$ is marked with thick blue line and $Re = 60$ with thick red line.

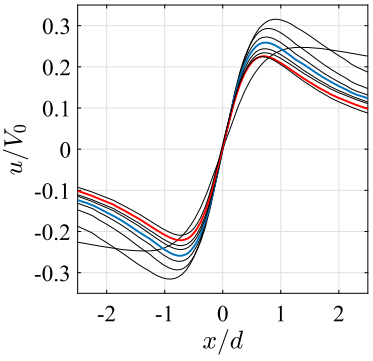

Figure 13: The u/V_0-velocity profiles at $y/d = 0.5$ for $Re \in \{1, 5, 10, 15, 20, 30, 40, 60, 80\}$ for the flow over one cylinder. The curve with smallest deviation from 0 is for $Re = 80$, and next curve corresponds to 60 and so one, except for one profile, the case of $Re = 1$, which intersects all other curves. The case of $Re = 20$ is marked with thick blue line and $Re = 60$ with thick red line.

one case, for example $Re = 20$, which is fast to simulate due to its steady features. Hence the results in the following text are extracted for $Re = 20$.

Flow over two cylinders

The flow over two cylinders is simulated with two configurations, tandem and side-by-side, illustrated in Figure 2. For the tandem configuration, the downstream cylinder has negligible effects on the upstream flow, resulting in similar upstream flow field as for one cylinder. The side-by-side configuration leads to new features, presented next.

The side-by-side configuration is studied by changing the surface spacing S. The normalized spacing is al-

tered among $g \in \{0.25, 0.5, 1, 3, 5, 10\}$. In Figure 15, the v-velocity profiles for the different spacings are shown. The profiles are plotted together with the sum of two one-cylinder profiles. For $g = 0.25$, the velocity profile resembles the form of the profile for one cylinder with larger diameter, however with some deviations at the center of the profile due to the hole between the cylinders. When the surface spacing increases, the profile starts to divide into two profiles, each increasingly resembling the shape of one cylinder with diameter d. For $g \geq 5$, the difference compared to the one-cylinder case is negligible. The same behaviour holds for the u-velocity.

The sum of the velocity fields of two single cylinders, where one field is translated such that the two cylinders are positioned with a spacing g, does not in general agree with the field of the corresponding two-cylinder configuration. This is clearly seen for small $g = 0.25, 0.5, 1$. For larger g, the summation is a reasonable approximation. This is however due to the fact that the behaviour of each of the two cylinders tends to the behaviour of one cylinder, together with the rapid decay of the impact from each cylinder away from the surface.

In Figure 14, the extreme value functions are plotted for $g = 0.5$. In general, the maximum value function of v, M_v, is similar to the one-cylinder case. The minimum value function, m_v, has however smaller values for the side-by-side configuration compared to the case for one cylinder, with decreasing discrepancies for increasing g. Already at $g = 3$, the difference is negligible.

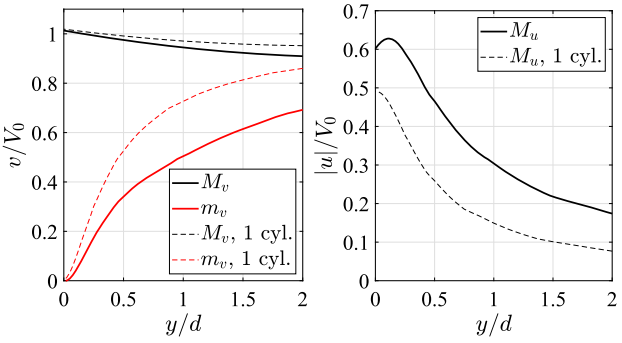

Figure 14: Extreme value functions for the flow over two cylinders side-by-side at $Re = 20$ and spacing $g = 0.5$. The dashed lines correspond to the case of one cylinder.

For M_u, the values are higher for the side-by-side configuration compared to the one-cylinder case for smaller g, this is seen in Figure 14 for $g = 0.5$. The curve tends to the one-cylinder case when g increases, however slower than for the v-velocity. Still at $g = 10$ there are small differences between the curves. This is due to the fact that the u-profile has a small asymmetry at each cylinder still present at large g, so the deviation from 0 is larger on the outside of the cylinders compared to in-between the two cylinders.

Flow over one row of cylinders

In Figure 16, the v-velocity profiles for different spacings $g \in \{0.25, 0.5, 1, 3, 5, 10\}$ are shown for the flow over one row of cylinders. Compared to the cases of one and two cylinders, the influence of a cylinder row leads to a maximum velocity clearly higher than the main stream velocity. This is logical since the total flow through the cylinder row is constant because of the fixed inlet velocity, requiring that the flow which is slowed down in front of the cylinders has to compensate by a larger velocity through the holes in between. Moreover, the reduction of the flow velocity away from the cylinders is not as strong as for the one-cylinder case. For instance with $g = 1$, the minimum v-value at $y/d = 0.25$ is about $0.55V_0$, compared to $0.3V_0$ for the one-cylinder case.

For small spacings $g = 0.25, 0.5, 1$, the reduction dip over each cylinder has a similar form as the magnified dip between the cylinders, but mirrored. This symmetry however disappears when the spacing increases ($g = 3, 5, 10$). Instead the increase in velocity between the cylinders, with a maximum value of almost $1.4V_0$ for $g = 0.25, 0.5, 1$, is reduced and smoothed out evenly over the gap. For $g = 3$, the maximum value at $y/d = 0.25$ is approximately $1.24V_0$, for $g = 5$ and $g = 10$ it is $1.17V_0$ and $1.07V_0$, respectively. When g increases, the reduction in front of the cylinders is increased. In Figure 17, the corresponding u-velocity profiles are shown.

An important difference between the row configuration and the one- and two-cylinder cases is seen when comparing the profiles for $g \leq 1$ at $y/d = 1$. The velocity profiles show that the flow is almost not affected at all at this short distance upstream. This implies that rows of cylinders have a shorter range of impact on the upstream flow field compared to one and two cylinders alone. Further, the amplitude of the impact depends on how close the cylinders are positioned. As for the case of two cylinders side-by-side, the profiles increasingly resemble the one-cylinder case when the spacing increases. However, for the v-velocity the resembling feature is slower compared to two cylinders. The same features are seen for the u-velocity, with the difference that the profiles gets similar to the one-cylinder case faster when g increases.

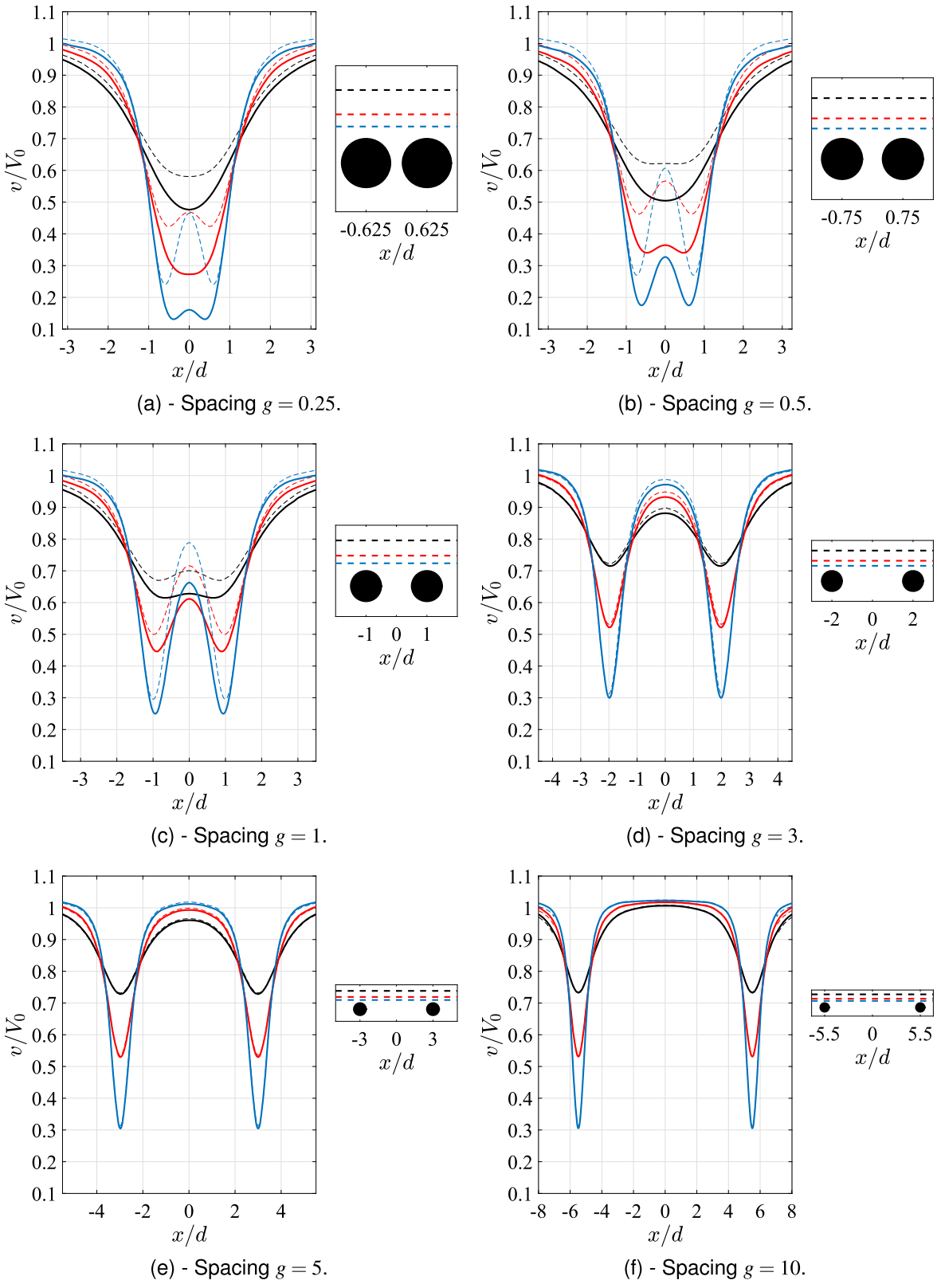

(a) - Spacing $g = 0.25$. (b) - Spacing $g = 0.5$.

(c) - Spacing $g = 1$. (d) - Spacing $g = 3$.

(e) - Spacing $g = 5$. (f) - Spacing $g = 10$.

Figure 15: Normalized velocity profiles v/V_0 for two cylinders side-by-side for different surface spacings g at $Re = 20$. Profiles are plotted at three different positions upstream, $y/d = 1$, $y/d = 0.5$ and $y/d = 0.25$. The dashed lines correspond to the sum of profiles of two single cylinders, positioned as two side-by-side cylinders.

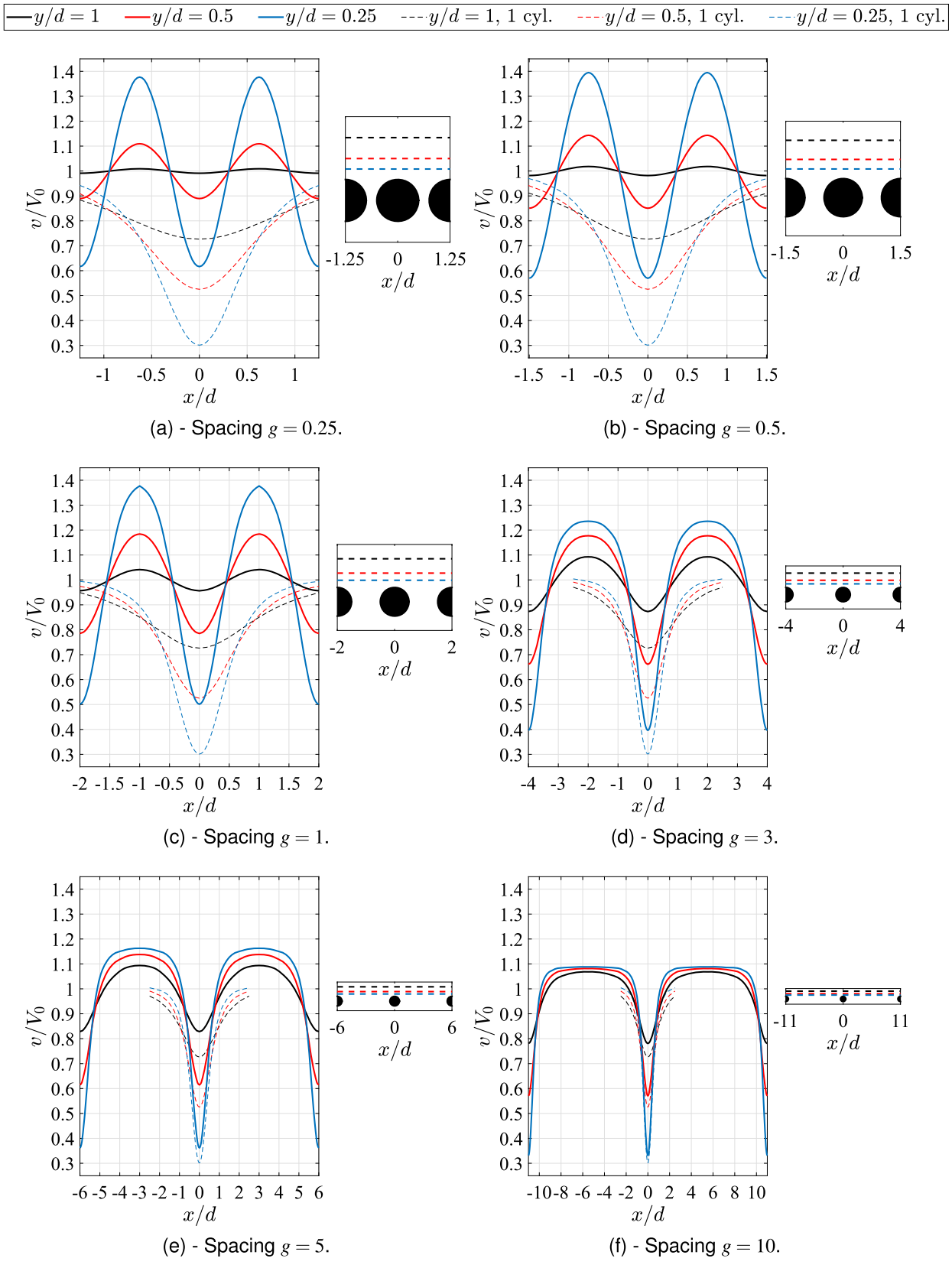

Figure 16: Normalized velocity profiles v/V_0 for the flow over one row of cylinders at $Re = 20$ for spacings $g \in \{0.25, 0.5, 1, 3, 5, 10\}$. The profiles are plotted at three different positions upstream, $y/d = 1$, $y/d = 0.5$ and $y/d = 0.25$. The dashed curves are the profiles for the one-cylinder case.

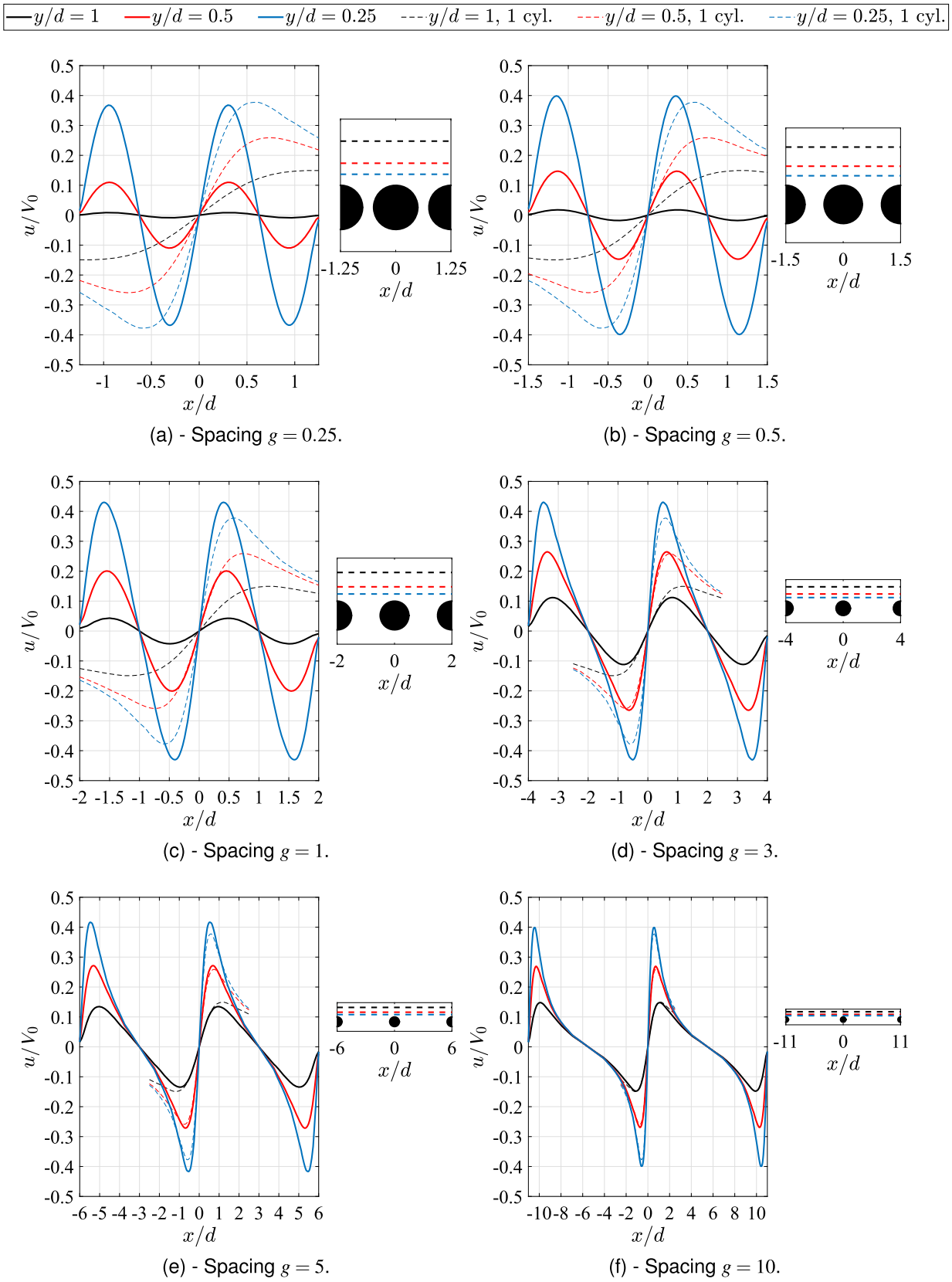

Figure 17: Normalized velocity profiles u/V_0 for the flow over one row of cylinders at $Re = 20$ for spacings $g \in \{0.25, 0.5, 1, 3, 5, 10\}$. The profiles are plotted at three different positions upstream, $y/d = 1$, $y/d = 0.5$ and $y/d = 0.25$. The dashed curves are the profiles for one cylinder.

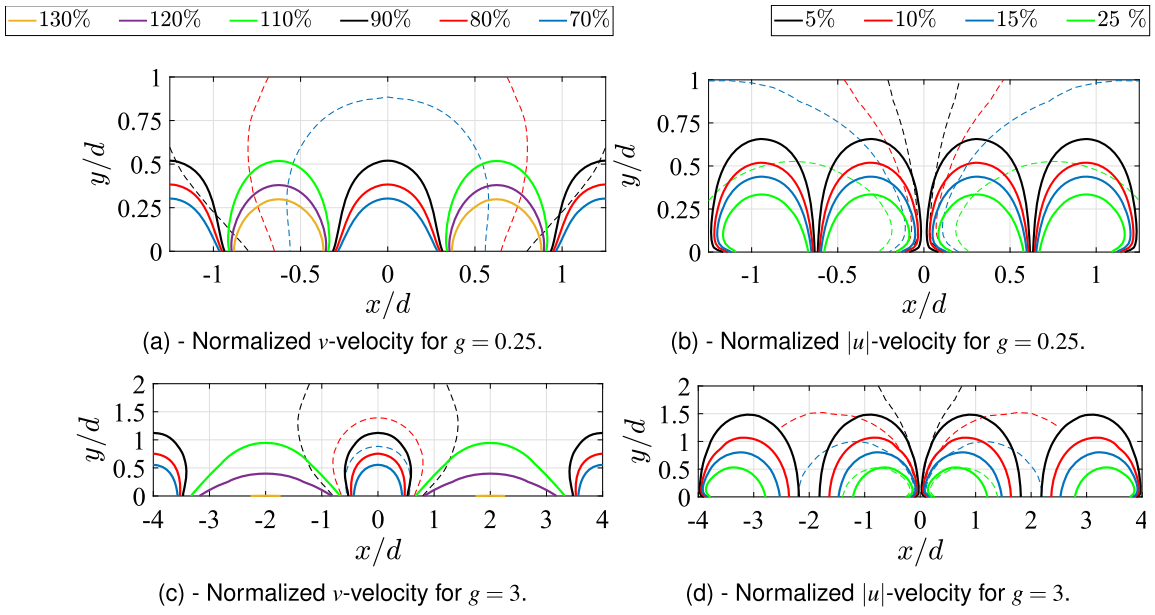

Figure 18: Level curves for the flow over one row of cylinders at $Re = 20$ for two different spacings $g = 0.25$ and $g = 3$. The dashed lines correspond to the case of one cylinder.

In Figures 19–20, the extreme value functions of v and u are plotted for $g = 0.25$ and $g = 3$, together with the extreme value functions for one cylinder.

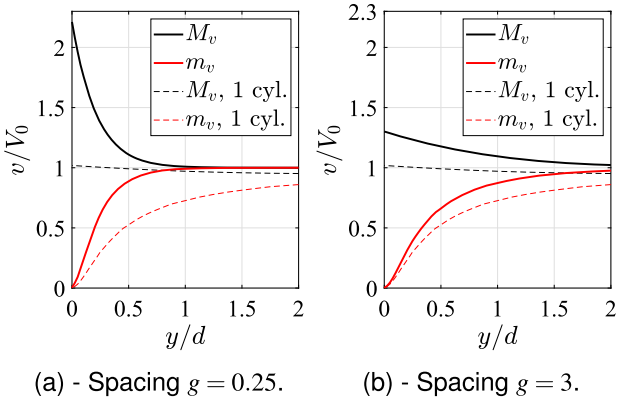

Figure 19: Extreme value functions for v for the flow over one row of cylinders at $Re = 20$ for two different spacings $g = 0.25$ and $g = 3$. The dashed lines correspond to the case of one cylinder.

In the case of v with $g = 0.25$, it is seen that the functions differ compared to the one-cylinder case. When g increases the functions increasingly resemble the one cylinder case, indicated by the plot for $g = 3$. For u, the maximum value is higher compared to the one-cylinder case close to the cylinder and decreases faster compared to the one-cylinder case when y/d increases.

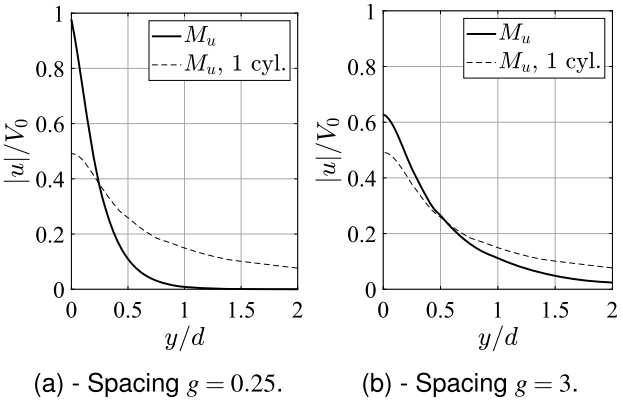

Figure 20: Extreme value function for u for the flow over one row of cylinders at $Re = 20$ for two different spacings $g = 0.25$ and $g = 3$. The dashed lines correspond to the case of one cylinder.

In Figure 18, the level curves for v and u at spacings $g = 0.25$ and $g = 3$ are plotted together with the one-cylinder case. Compared to the level curves for the one-cylinder case, it is a significant difference in size of the regions affected.

As for the one-cylinder case, the Reynolds number dependency is investigated for the row case. The conclusion is the same. There is a change in the velocity profiles when the Reynolds number is changed but the profiles keep the similar shape in the range $Re \in [10, 80]$, with smaller deviations from the main stream velocity for larger Reynolds numbers. The effect from the unsteady flow is small, less

than 2 % point-wise deviations from the mean velocity profile for $Re = 60$.

Flow over two rows of cylinders

The flow over two rows of cylinders is investigated for two configurations, tandem and displaced. Two surface spacings are varied, the spacing $g = S_x/d$, between the cylinders in each row, and the spacing $l = S_y/d$, between the two rows. The value of g is chosen as $g \in \{0.25, 0.5, 1, 3, 5, 10\}$, and $l \in \{0.1, 0.5, 1, 3, 5\}$. The upstream differences between two rows tandem and one row are negligible, as was the case when comparing one cylinder to two tandem cylinders. However, for the displaced configuration, new features occur.

In Table 1, an overview of all different displaced setups for two rows of cylinders is shown, indicating whether the velocity profiles differ compared to the one-row case or not. The differences from the visual comparison is expressed by three different abbreviations, S, MD, or D, where S indicates that the profiles are very much the same, MD indicates a minor difference, and D indicates that the profiles are clearly different.

Table 1: Results of visual comparison of the v-velocity profiles (differences for u indicated in parenthesis) for the flow over two rows of cylinders in the displaced configuration at $Re = 20$ for different values of g and l. The profiles are compared with the one-row case and visual differences are indicated in three ways: D - difference, MD - minor difference, S - similar.

$l \backslash g$	0.25	0.5	1	3	5	10
0.1	S	S	S	D	D	D
0.5	S	S	S	D (MD)	D	D
1	S	S	S	MD (S)	D (MD)	D
3	S	S	S	S	MD (S)	D (MD)
5	S	S	S	S	S	MD (S)

In Figures 21–22, the v- and u-velocity profiles for spacings $g = 5$ and $l = 0.1, 1, 3$ are shown. By observing the table and the profiles, it can for example be seen that for v with $g = 5$ and $l = 1$, there is a difference (D) compared to the one-row case, but for u the difference is only minor (MD).

There are no differences for the smallest spacings, $g = 0.25, 0.5, 1$, compared to the one-row case. This implies that when the cylinders in each row are positioned close together, the second row has no effect on the upstream velocity profile, no matter the spacing between the rows, or

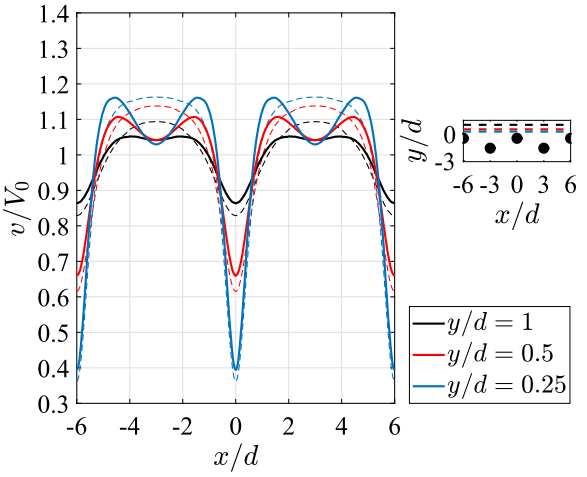

(a) - Spacings $g = 5$ and $l = 0.1$.

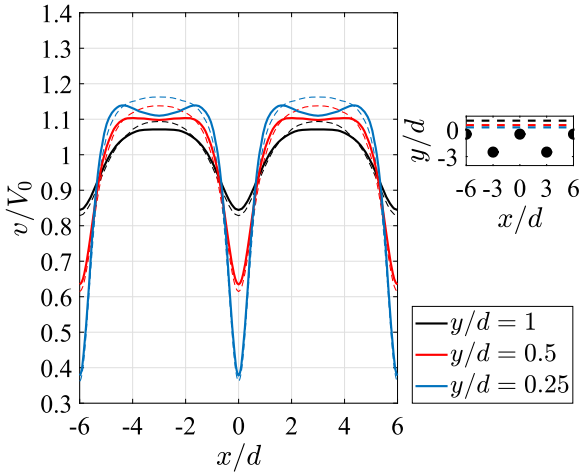

(b) - Spacings $g = 5$ and $l = 1$.

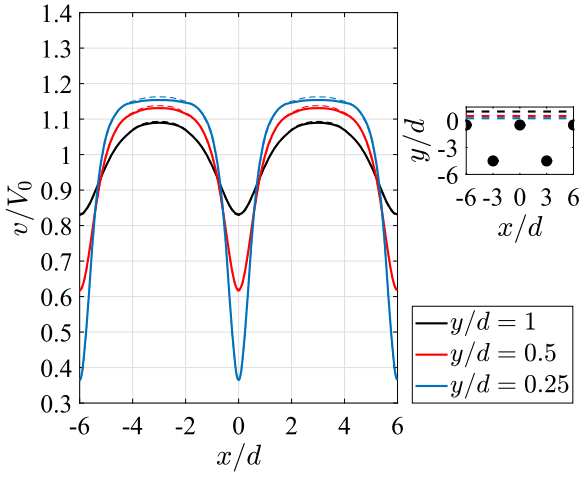

(c) - Spacings $g = 5$ and $l = 3$.

Figure 21: Normalized velocity profiles for v/V_0 for the flow at $Re = 20$ over two rows of cylinders where the second row is displaced. Three setups are shown, $g = 5$ and $l \in \{0.1, 1, 3\}$. The dotted lines show the profile for the flow over one row of cylinders.

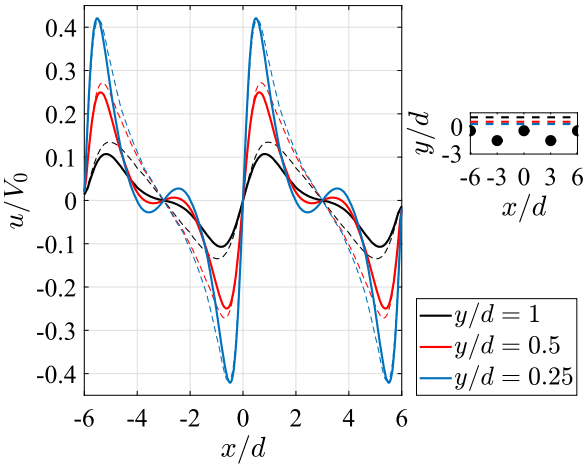

(a) - Spacings $g = 5$ and $l = 0.1$.

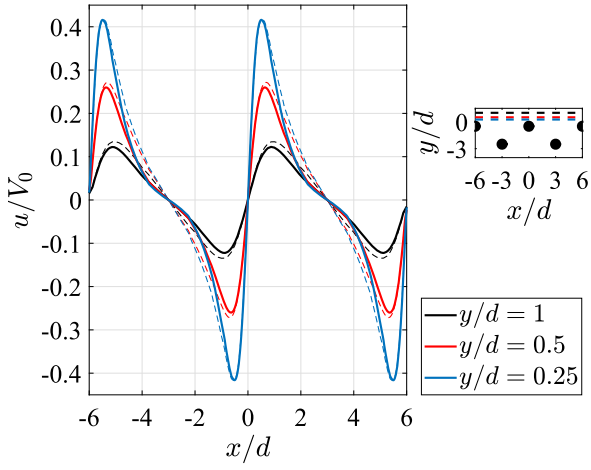

(b) - Spacings $g = 5$ and $l = 1$.

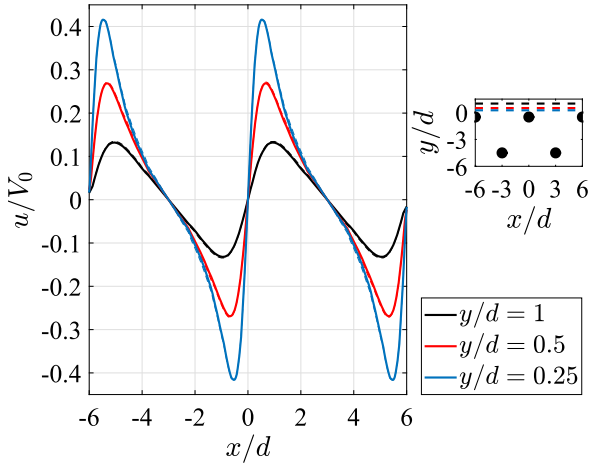

(c) - Spacings $g = 5$ and $l = 3$.

Figure 22: The normalized velocity profiles for u/V_0 for the flow at $Re = 20$ over two rows of cylinders where the second row is displaced. Three setups are shown, $g = 5$ and $l \in \{0.1, 1, 3\}$. The dotted lines show the profile for the flow over one row of cylinders.

if the second row is displaced. Between $g = 1$ and $g = 3$ the second row starts to influence the upstream flow. This impact however decreases when the spacing between the rows, l, increases.

In Figure 21, the v-velocity profiles for $g = 5$ and $l = 0.1, 1, 3$ show how the typical influence on the velocity profile is manifested. There are dips in the profile from the reduced velocity due to the cylinders in the second row. For $l = 0.1$ and $l = 1$, the second row reduces the impact of the flow at $y/d = 1$, implying that a second row can be used to reduce the upstream range of impact. When l increases, the profiles increasingly resemble the case of one row of cylinders.

The differences between the displaced two-row configuration and the one-row configuration which is seen in the velocity profiles, cannot be seen when plotting the extreme value functions. This is due to the fact that the maximum and minimum values of the velocity profiles are not differing much compared to the one row case, even though the shapes differ. This can be seen by comparing the profiles in Figures 21–22.

For the level curve analysis, the results resemble in much accordance the results seen in Table 1 for the velocity profiles. This is exemplified in Figure 23 for the v- and u-velocity at $g = 3$. For v it can be seen that the regions where the velocity is decreased are similar to the corresponding regions for the one-row cylinder configuration. The largest difference is instead observed for the regions where the main stream velocity is reduced.

Measures of upstream flow impact

In this section, all three configurations of rows: one row, two rows tandem, and two rows displaced, and all their different subsetups, are compared together. This overall comparison is accomplished by analysing the pressure drop and three upstream impact measures: a length-measure, an area-measure and a variation-measure. The length-measure is the length upstream for which the velocity field is deviating more than a certain threshold. The area-measure is the area upstream where the velocity is deviating from the main stream velocity more than a certain threshold, given per cylinder, only counting cylinders in the first row. Lastly, the variation-measure is the difference between the maximum and minimum velocity. In the following paragraphs these measures are defined precisely.

To define the area- and length-measures, the following two indicator functions are introduced, one for each

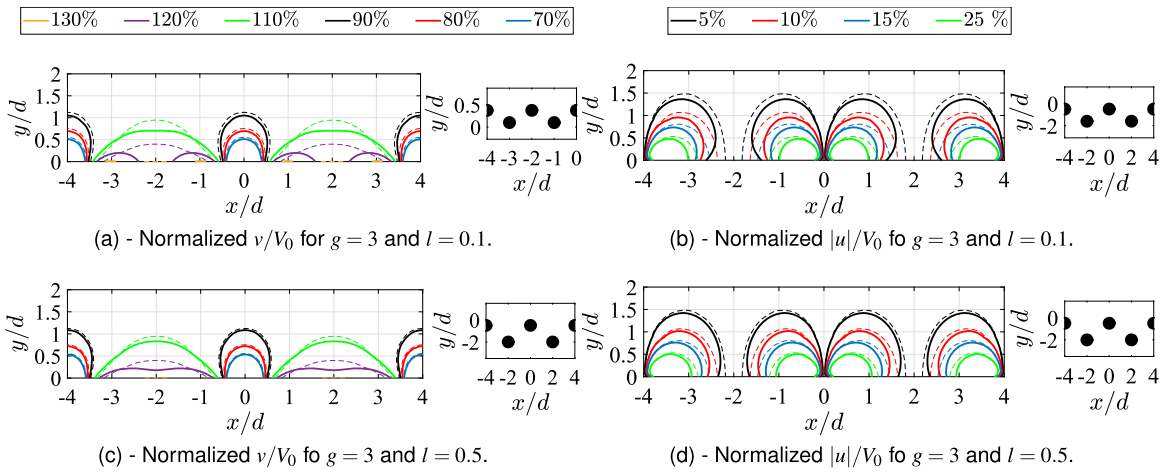

(a) - Normalized v/V_0 for $g = 3$ and $l = 0.1$.

(b) - Normalized $|u|/V_0$ fo $g = 3$ and $l = 0.1$.

(c) - Normalized v/V_0 fo $g = 3$ and $l = 0.5$.

(d) - Normalized $|u|/V_0$ fo $g = 3$ and $l = 0.5$.

Figure 23: Level curves for the flow over two rows of cylinders with one row displaced at $Re = 20$. Two setups are shown, with spacings $g = 3$ and $l \in \{0.1, 0.5\}$. The dotted lines correspond to the one-row case.

velocity component:

$$I_a^v\left(\frac{x}{d},\frac{y}{d}\right) = \begin{cases} 1, & \text{if } \left|\frac{v(x,y)}{V_0} - 1\right| \geq a, \\ 0, & \text{else,} \end{cases} \tag{7}$$

$$I_a^u\left(\frac{x}{d},\frac{y}{d}\right) = \begin{cases} 1, & \text{if } \left|\frac{u(x,y)}{V_0}\right| \geq a, \\ 0, & \text{else,} \end{cases} \tag{8}$$

where a is the threshold value. The area-measure A_a^Γ, where $\Gamma \in \{u, v\}$, is defined as

$$A_a^\Gamma = \frac{1}{n} \iint\limits_{\mathbb{R}\times\mathbb{R}^+} I_a^\Gamma(s,t)\, dsdt, \tag{9}$$

where n is the number of cylinders in the first row. For the row configurations, the integral will be finite because of periodicity of the flow field.

The length-measure L_a^Γ, $\Gamma \in \{u, v\}$, is defined as

$$L_a^\Gamma = \sup\left\{\frac{y}{d} : I_a^\Gamma\left(\frac{x}{d},\frac{y}{d}\right) = 1 \text{ for some } x \in \mathbb{R}_+\right\}. \tag{10}$$

To measure the variation of the flow field, the difference between the maximum and minimum value of a velocity component is investigated. For this purpose, variation functions $D^v(\cdot)$ and $D^u(\cdot)$, are defined according to

$$D^v\left(\frac{y}{d}\right) = \max_{x\in\mathbb{R}} \frac{v(x,y)}{V_0} - \min_{x\in\mathbb{R}} \frac{v(x,y)}{V_0}, \tag{11}$$

$$D^u\left(\frac{y}{d}\right) = \max_{x\in\mathbb{R}} \frac{|u(x,y)|}{V_0}. \tag{12}$$

For the v-velocity, the variation functions can be related to the length-measure by considering the variation at the upstream position L_a^v, denoted by

$$D_a^v = D^v(L_a^v). \tag{13}$$

Next, the different measures are calculated and compared for different cylinder configurations.

In Figure 24, the pressure drops for the different row cylinder configurations are shown at $Re = 20$. A dashed line corresponding to slope $k = -1.5$ is included to indicate the rate of decrease of the pressure drop when the surface spacing g increases.

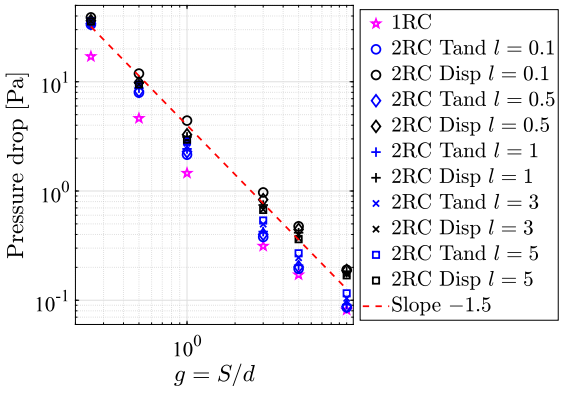

Figure 24: Pressure drop for the different cylinder configurations at $Re = 20$. The dashed red line corresponds to a slope of $k = -1.5$.

These results show that for $Re = 20$, the pressure drop depends non-linearly on g. Hence, Darcy's law (Bird et al. 2002) is not valid for our application. Darcy's law is sometimes used to model the flow through paper, but as the pressure drop plot shows, the zero inertia approximation is not valid. Therefore, for fabric flow, Navier-Stokes based simulations are required. Moreover, cylinder configurations and forming fabrics may not necessary be regarded

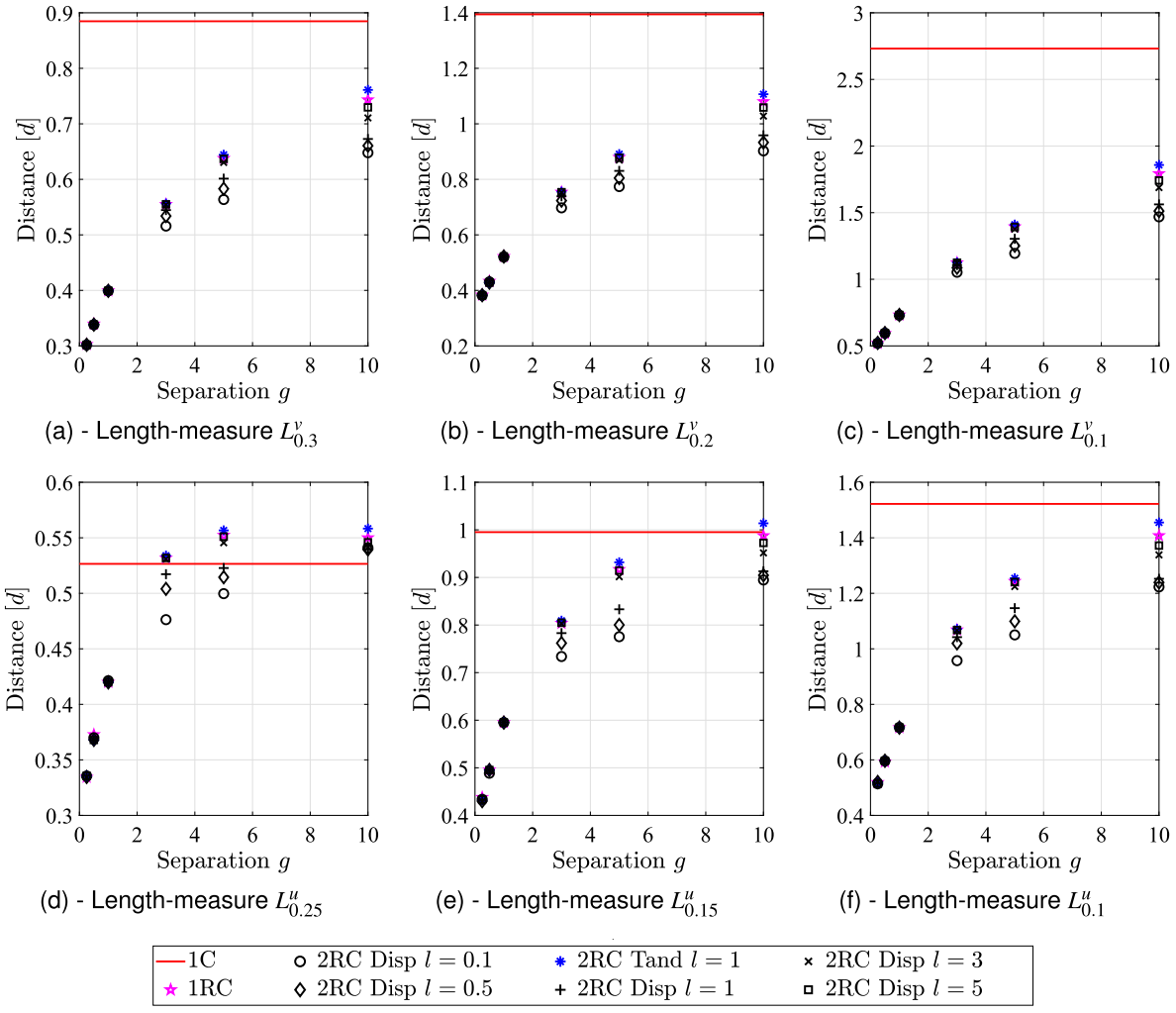

Figure 25: The length-measure L^Γ_a for the flow over different cylinder configurations at $Re = 20$. Only one row spacing for two rows in tandem is included, $l = 1$.

as a continuum, which is the assumption that Darcy's law is based on. Regardless, the factor $k = -1.5$ shows what rate of decrease of the pressure drop that can be expected when varying the surface spacing for these cylinder configurations.

In Figure 25, the different configurations are compared using the length-measure L^Γ_a. There are six plots, three for v and three for u. For v, the thresholds are chosen as $a = 0.3, 0.2, 0.1$ and for u, the corresponding values are $a = 0.25, 0.15, 0.1$. In all plots, the different row configurations and their subsetups are included, also the value for one cylinder is included.

The row configurations give up to 65 %, 71 % and 82 % shorter impact range for the v-velocity compared to one cylinder for threshold value $a = 0.3$, $a = 0.2$ and $a = 0.1$, respectively. Smaller surface spacing g leads to shorter impact range. For $g = 0.25, 0.5, 1$, the different row configurations do not depend on the spacing l between the rows. Somewhere between $g = 1$ and $g = 3$, the displaced configuration starts to depend on l, and the difference between different l-values increases with g. This result indicates that a displaced second row reduces the upstream impact, but only for g larger than one diameter.

In Figure 26, the area-measure A^Γ_a is plotted for $a = 0.25, 0.15, 0.10$. For spacings $g = 0.25, 0.5, 1$, the area-measure for the row configurations is over 50 % smaller compared to the one-cylinder configuration. Similarly as for the length-measure, there is no dependency on l for $g = 0.25, 0.5, 1$. For larger spacings $g > 1$, the dependency on l is different for different a-values.

In Figure 27, the variation-measure $D^\Gamma(y/d)$ is shown for three different positions upstream, $y/d = 0.25, 0.5, 1$. For $y/d = 0.25$ the variation-values are larger compared to the one-cylinder case, while for $y/d = 1$, the values are

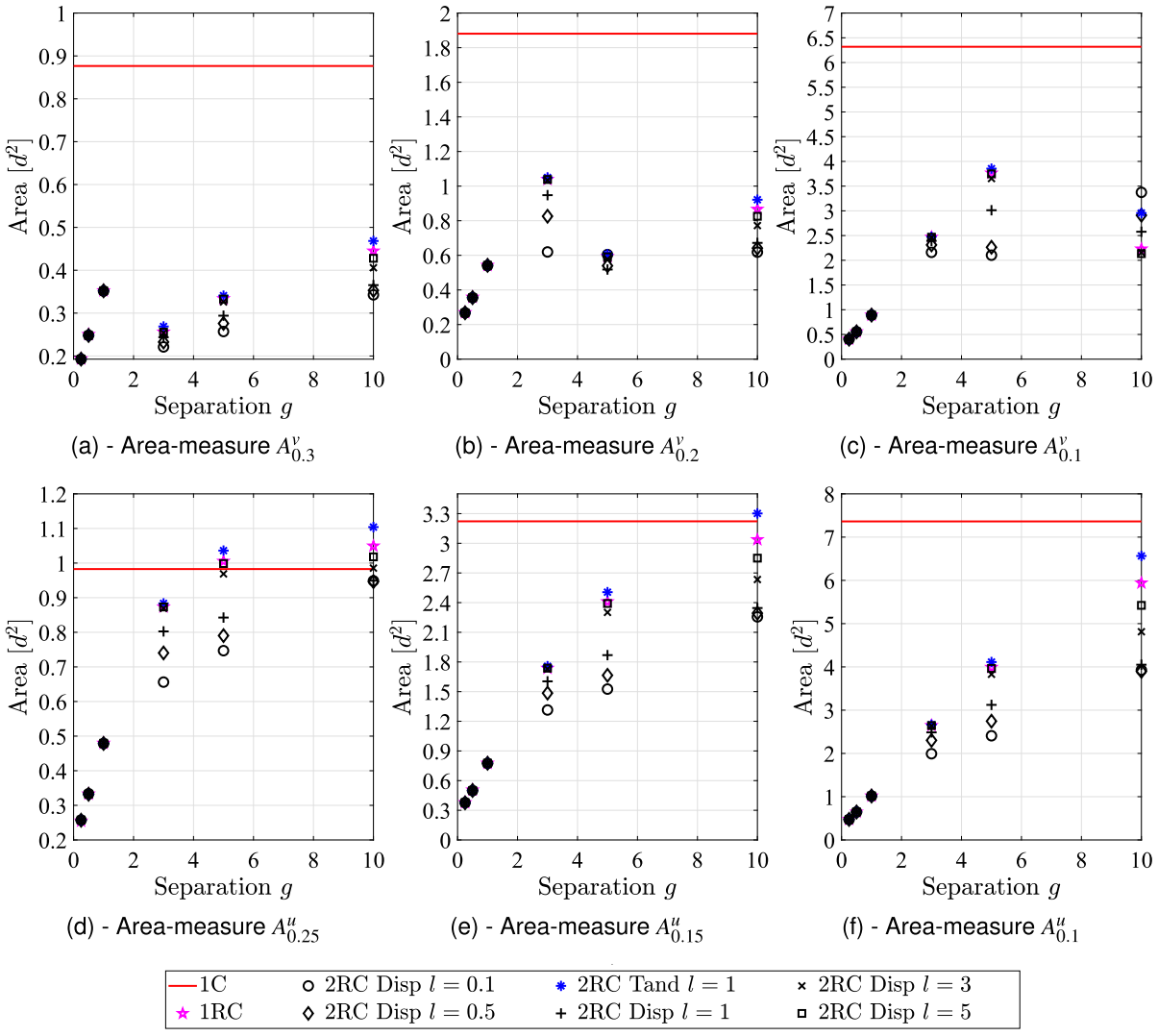

Figure 26: The area-measure A^{Γ}_{a} for the flow over different cylinder configurations at $Re = 20$. Only one row spacing for two rows in tandem is included, $l = 1$.

smaller for almost all setups. For $y/d = 1$, the dependency on l is negligible for $g = 0.25, 0.5, 1$. However, there is a weak dependency on l for $y/d = 0.25$ and $y/d = 0.5$.

Fabric flow characteristics

The air flow over three different forming fabrics and the resulting volume flow per area is presented in the Validation section, showing excellent agreement with experiments. The volume flow per area is expressed in the unit CFM, which is common when comparing flow characteristics of fabrics. However, as is suggested next, the CFM-measure alone is not sufficient to describe fabric flow properties. Therefore additional measures, such as the ones introduced in the previous section, are needed.

The fabrics in this study have the following CFM-values at a pressure drop of 125 Pa: Fabric A, 388 CFM, Fabric B, 388 CFM, and Fabric C, 352 CFM. The values are listed in Table 2. The CFM-measure indicates that Fabric A and Fabric B have similar flow characteristics while Fabric C differs 10 %. If the pressure drop is varied the mutual difference is similar (see Figure 5).

In Figure 28, snapshots of the top layer of the three fabrics are shown. The area void fraction ϕ, defined as the percentage empty space, is calculated from the snapshots using image analysis tools. The resulting values are: $\phi_A = 0.16$, $\phi_B = 0.27$, and $\phi_C = 0.28$. The indication based on the CFM-measure, that Fabric A and Fabric B are similar, is not strengthened through the visual comparison of the top layers of the fabrics. The difficulty of character-

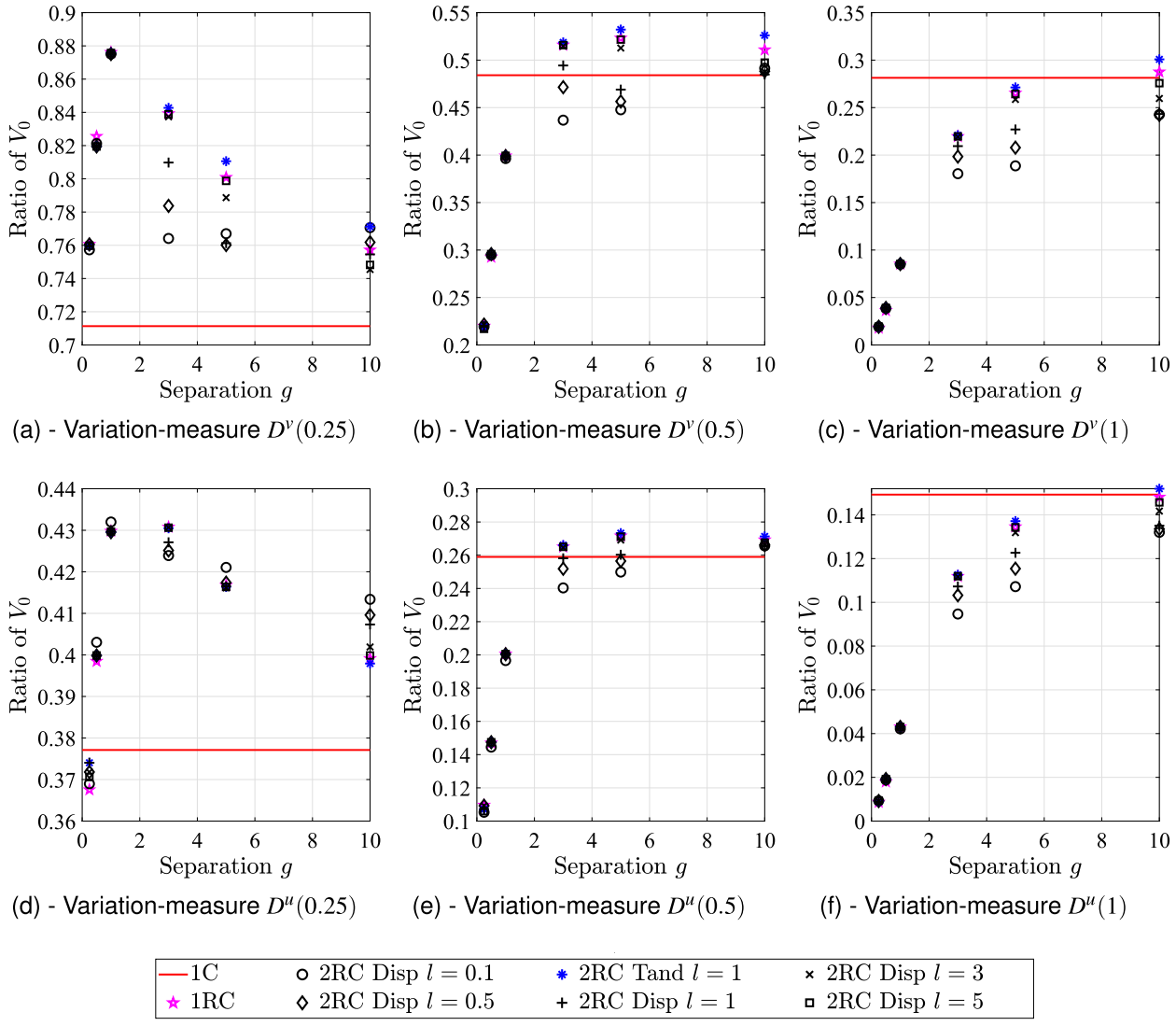

Figure 27: The variation-measure $D^{\Gamma}(y/d)$ for the flow over different cylinder configurations at $Re = 20$. Only one row spacing for two rows in tandem is included, $l = 1$.

ising flow properties of fabrics, by only considering the CFM-measure, is thereby demonstrated. To broaden the characterization, the length-measure L_a^v and the variation-measure D^v, introduced in the previous section, are employed.

To compare the fabrics based on the length- and variation-measure, the air flow is simulated using fixed inlet velocity, with $Re = 20$, calculated from the top layer diameter. The top layer threads of Fabric A have diameters 0.15 mm and 0.17 mm. For Fabric B, the diameters are 0.12 mm and 0.13 mm, and for Fabric C, the diameter is 0.11 mm. For the fabrics with two different diameters, the mean value is used to calculate the Reynolds number.

The length-measure L_a^v is calculated for $a = 0.1$, 0.2, 0.3, and the variation-measure $D^v(y/d)$ for $y/d = 1$, 0.5, 0.25. The results are presented in Table 2. Note that the values are calculated with normalization based on the mean diameter and the main stream velocity, which both are different for the three fabrics.

The $L_{0.1}^v$-values for Fabric B and Fabric C differs less than 2 %. However, a larger difference occur for $a = 0.2$, and the mutual order of increase between all three fabrics, which are the same for $a = 0.1$ and $a = 0.2$, changes for $a = 0.3$. For the variation-measure, the values of Fabric B and Fabric C at $y/d = 1$ differ less than 2 %. For $y/d = 0.5$, the difference is over 10 %. At $y/d = 0.25$, the values for Fabric A and Fabric C are similar. These tendencies indicate that the length-measure and the variation-measure describe more aspects than the CFM-measure. However, at this point the reasons behind are unclear. To understand

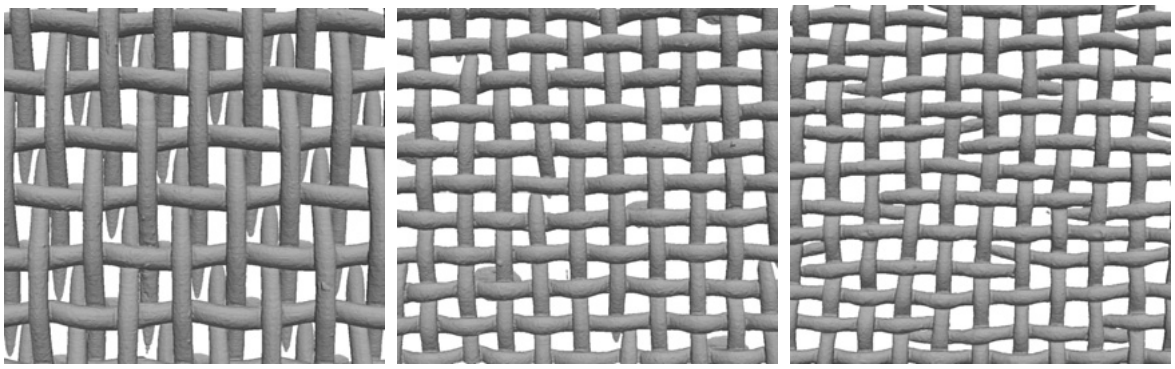

(a) - Fabric A (b) - Fabric B (c) - Fabric C

Figure 28: The top layer for each of the three fabrics. Size is 2.9 mm × 2.7 mm ($x \times y$).

Table 2: A list of different measures of the three forming fabrics. The measures are in the following order: the CFM-measure, the approximated g-value, the length-measure L_a^v for three different a-values and the corresponding variation-measure D_a^v at these positions upstream, and the variation-measure $D^v(y/d)$ for three different distances upstream. All values are normalized with V_0 and the mean diameter. The flow is simulated at $Re = 20$.

(Normalized)	Fabric A	Fabric B	Fabric C
CFM (125 Pa)	388	388	352
g	0.67	1.08	1.12
$L_{0.1}^v$	2.28	2.99	3.05
$L_{0.2}^v$	1.30	1.52	1.75
$L_{0.3}^v$	0.84	1.14	1.00
$D_{0.1}^v$	0.15	0.17	0.18
$D_{0.2}^v$	0.32	0.34	0.35
$D_{0.3}^v$	0.54	0.48	0.57
$D^v(1)$	0.45	0.58	0.57
$D^v(0.5)$	0.85	1.03	0.89
$D^v(0.25)$	1.24	1.35	1.26

some of the differences, the resulting values of L_a^v and D^v are related to the results of the cylinder study.

Before comparing the results of the cylinder study and the fabric results, it should be stressed that the cylinder configurations considered in this work are not only a simplification of a forming fabric to two dimensions, but moreover the study was restricted to uniform diameter of the cylinders, uniform displacements between the cylinders, and regular configurations. Forming fabrics violate these conditions to various extent: they are three-dimensional with varying thread diameters and a complex weaving pattern resulting in non-uniform spacings and displacements. In the following discussion, the results from the cylinder study are extrapolated to the three fabrics.

Using the area void fraction ϕ, and the following geometrical argument, approximative values of g can be attained for the three forming fabrics. For a fabric with a uniform grid pattern as in Figure 29, with cylinder diameter d and normalized spacing between the cylinders denoted g (defined as before), the void fraction is given by the formula

$$\phi = \frac{g^2}{g^2 + 2g + 1}. \tag{14}$$

By inverting this formula, the g-values for the three fabrics are calculated, with values $g_A = 0.67$, $g_B = 1.08$, and $g_C = 1.12$. Based on what was concluded from the cylinder study, this implies that the effects from the second row are very small, no matter the row spacing l or the displacement of the second row. Hence only the top layer is considered when analysing the relation between the fabric structure and the length-measure and variation-measure. It should be remembered that the diameters of the threads in the second layer are different to the threads in the first layer, which can give effects not captured by the cylinder study.

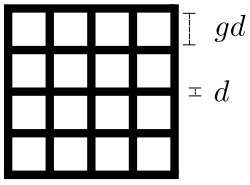

Figure 29: Illustration of a simple regular weaving pattern.

For all three values of a, the length-measure is higher than what was seen in the cylinder study (compare Figure 25). If this if due to three dimensions, or related to

some of the other violating conditions of the fabrics is unclear and an open question. However, for the small impact threshold $a = 0.1$, Fabric A has about 26 % smaller value compared to Fabric B and Fabric C. From the cylinder study it was concluded that when g is smaller, the impact range decreases. Accordingly, this is likewise true for the different fabrics. Based on this, low impact range can be achieved by constructing fabrics with small value of g.

For Fabric B and Fabric C, whose g-values only differ about 4 %, the length-measure shows interesting tendencies. For $a = 0.1$ and $a = 0.2$, Fabric C has the highest length-measure values, which corresponds to its marginally higher g-value. However, for the high impact value $a = 0.3$, Fabric B has a higher length-measure value. The reason for this is unclear and difficult to explain based on the two-dimensional cylinder study. This feature may be related to the irregularity of the threads of Fabric C, or to that Fabric B has varying thread diameters in the top layer.

Considering the variation-measure D^v, all values are higher for the forming fabrics compared to the cylinder configurations, similarly as was the case for the length-measure. This is likely due to the same reasons, which was discussed for the length-measure. As was seen in the cylinder study, a smaller g-value gives smaller variation, which holds true for the forming fabrics. Fabric A, which has the smallest g-value, has the smallest variation-measure for all three positions upstream y/d. Similarly as for the length-measure analysis, the variation-measure shows interesting trends for smaller y/d. For instance, Fabric A and Fabric C have similar values for $y/d = 0.5$ and $y/d = 0.25$, while Fabric B and Fabric C, whose values are similar for $y/d = 1$, differs for $y/d = 0.5$ and $y/d = 0.25$.

The preceding discussion is based on analysing the normalized values of the measures, which is appropriate when comparing the fabric results to the cylinder results. However, since the diameters are different for the three fabrics, absolute values give a different view, which is equally relevant. Next, the absolute values are discussed.

Using an inlet velocity of 2 m/s for all three fabrics, the flows are simulated, and the measures are calculated with absolute values. The results are presented in Table 3. The absolute values of the measures are now discussed in relation to the description of the fabrics, given in the Method section.

Comparing the values of Fabric A with Fabric C, where Fabric C in many cases has replaced Fabric A in production, it is seen that Fabric C has marginally shorter impact range and smaller variation values. This shows that Fabric C gives slightly better flow properties than Fabric A, with increased uniformity of the flow field. The advantage of Fabric C compared to Fabric A, its longer wear resistance, is not part of this study.

Table 3: A list of different measures of the three forming fabrics. The measures are in the following order: the CFM-measure, the approximated g-value, the length-measure L_a^v for three different a-values and the corresponding variation-measure D_a^v at these positions upstream, and the variation-measure $D^v(y/d)$ for three different distances upstream. Absolute values for the measures are given in mm and m/s. The flow is simulated with an inlet velocity $V_0 = 2$ m/s for all three fabrics.

(Absolute)	Fabric A	Fabric B	Fabric C
CFM (125 Pa)	388	388	352
gD	0.11 mm	0.14 mm	0.12 mm
$L_{0.1}^v$	0.36 mm	0.39 mm	0.35 mm
$L_{0.2}^v$	0.21 mm	0.20 mm	0.21 mm
$L_{0.3}^v$	0.13 mm	0.15 mm	0.12 mm
$D_{0.1}^v$	0.30 m/s	0.34 m/s	0.35 m/s
$D_{0.2}^v$	0.64 m/s	0.68 m/s	0.69 m/s
$D_{0.3}^v$	1.07 m/s	0.98 m/s	1.12 m/s
$D^v(0.15\text{ mm})$	0.96 m/s	0.94 m/s	0.93 m/s
$D^v(0.075\text{ mm})$	1.76 m/s	1.90 m/s	1.58 m/s
$D^v(0.0375\text{ mm})$	2.50 m/s	2.66 m/s	2.28 m/s

Fabric B has up to 10–20 % higher values compared to Fabric C, especially for the variation-measure. This indicates that Fabric B gives a higher impact range and less uniform flow field compared to the other two fabrics. This is in accordance with the fact that Fabric B is used for coarser packaging boards, while Fabric A and Fabric C are used for finer paper.

Finally, flow patterns which lead to a risk of drainage marking is investigated. In Figure 30, the z-velocity fields at an upstream position of $z = 0.15$ mm from the fabric surface are shown for the three forming fabrics. In Figure 31, the z-velocity profiles for the three fabrics are plotted. The z-direction is perpendicular to the fabric plane and similarly as for the cylinder flows the z-velocity is defined to be positive in the negative z-direction.

Wire marks are often divided into two types, those caused directly by the threads of the fabric, and those caused indirectly by the drainage channels of the fabric flow field. The second type is what is referred to as drainage marking. To reduce the risk of drainage marking, a periodicity of the flow with high wave length is undesirable, which often leads to design of fabrics with small threads in the top layer. However, as is discussed below, this does not necessarily lead to a reduced wave-length, since the second layer is also important.

In the field plots, it can be seen that the fabrics have different periodic flow patterns. The periodic pattern of

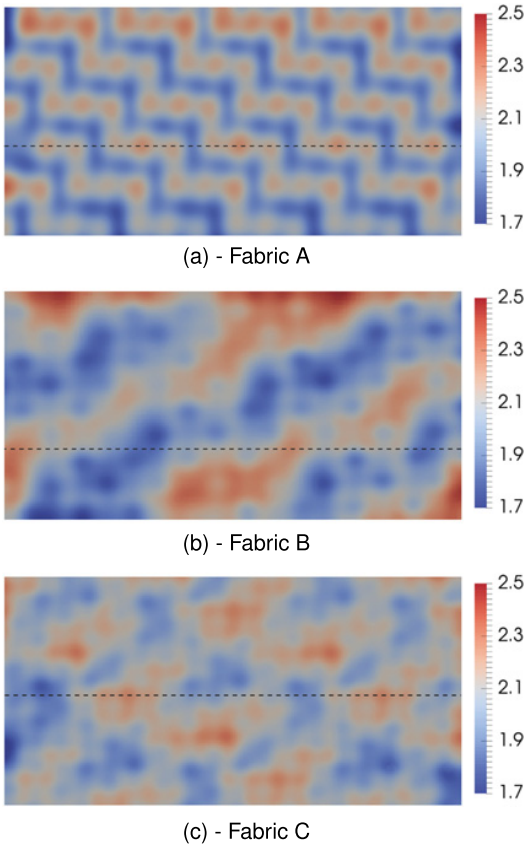

Figure 30: Upstream z-velocity field at position $z = 0.15$ mm over the fabric surface. Inlet speed is 2 m/s in negative z-direction. The dimension is 5.2×2.6 mm^2. The black dashed lines indicate where the velocity profiles in Figure 31 are extracted.

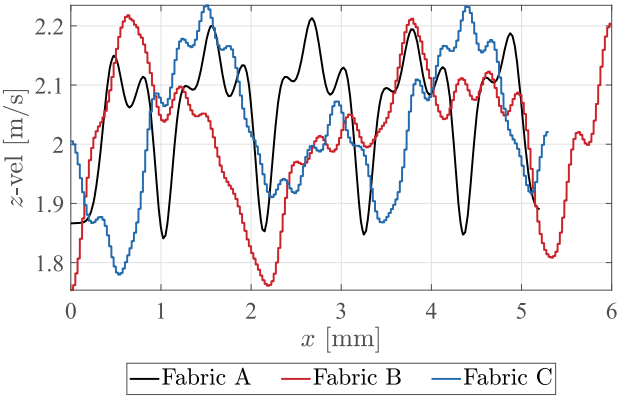

Figure 31: Upstream z-velocity profile extracted in a line parallel to the x-axis at position $z = 0.15$ mm over the fabric surface. Inlet speed is 2 m/s in negative z-direction. In Figure 30, it is indicated where in the x-y-plane the profiles are extracted.

Fabric B has a higher wave-length, which is seen in Figure 31. By comparing the wear side of Fabric B in Figure 3 with the flow field in Figure 30, it is seen that the diagonal reduction of the z-velocity coincides with the positions where the thick threads of the bottom layer go up and touch the top layer. Apparently the second layer affects the upstream flow. If this is due to the larger thread diameter, or that the spacing to the top layer at these points actually is zero, or a combination of these two, is an open question. Neither of these properties were investigated in the cylinder study. Moreover, this study shows that wave-length is another feature which is important to consider when constructing fabrics, since a high wave-length may increase the risk of drainage marking.

Conclusions

The objective of this work is to increase the understanding of the fundamentals of forming fabric flow. This is achieved by numerical investigation of the upstream flow over different cylinder configurations in the Reynolds number range typical for the forming process in a paper machine. Uniform cylinder diameter and uniform displacement between cylinders are assumed. Moreover, new measures for characterization of the upstream flow impact are proposed. Three industrial forming fabrics are studied and the results are compared with the cylinder study using the new impact measures.

The major conclusions of the cylinder study can be divided into three issues. Firstly, how far upstream the flow is affected due to the cylinders. Secondly, how variations in Reynolds number in the investigated range, 10–80, affect the upstream characteristics, and lastly, how the different configurations, and the surface spacings between cylinders, influence the flow features.

As is demonstrated in the result section, the upstream range of impact of the flow over cylinders is short. For example, the v-velocity upstream of the flow over one cylinder is reduced more than 30 % of the main stream velocity only in a region with a size approximately the same as the cylinder. Rows of cylinders, lead to an even further reduced range of impact, and with small spacings $g \leq 1$ between the cylinders in each row, the corresponding 30 % reduction region only ranges less than 0.4 cylinder diameters upstream.

Regarding the Reynolds number dependency, the simulation results show that for $Re \in [10, 80]$, the upstream characteristics are not changed when the Reynolds number is varied. This is surprising since the flow features downstream are changed essentially when the flow goes from steady to unsteady around $Re = 40$. The unsteadiness is merely observed upstream with deviations from the av-

erage velocity less than 2 %. The velocity profiles upstream are changed when the Reynolds number is increased, following the trend seen in Figure 12, with a shift upwards. However, the characteristic shape of the curve is the same for all Reynolds number in the interval 10–80, leading to a conclusion that it is enough to study upstream features at one single Reynolds number in the range 10–80, for example $Re = 20$, as in this paper.

The cylinder configurations studied are one cylinder, two cylinders tandem and side-by-side, one row, and two rows tandem and displaced. For the cases with multiple cylinders, the surface spacing is altered to investigate the influence on the upstream features. A main conclusion is that the tandem configurations do not introduce any distinct effect on the upstream flow features. However, a displaced second row may for certain configurations have an impact upstream. For small g (= 0.25, 0.5, 0.1), the second row does not influence the upstream flow, not even if displaced. For larger g, the range of impact upstream is decreased with a closely located second row. When the spacing l is increased, the influence from the second row is reduced. In general, for all multiple cylinder cases, when the spacing g increases, the flow tends to the one-cylinder case.

Investigation of the pressure drop for the row configurations leads to the conclusion that the pressure drop dependency on the porosity as well as the spacing g is non-linear. The required pressure drop for the displaced two-row configurations is about twice the value for one row. The same is true for two rows tandem but only for small $g = 0.25,\ 0.5,\ 1$. The pressure drop dependency on l is weak compared to g. The non-linear finding is important and could be used in forming fabric design.

In addition to the cylinder study, the flow characteristics of three different industrial forming fabrics are studied. The impact measures defined in this work are calculated and the fabric results are compared with the cylinder study. The results show that the fabrics follow the trends of the cylinders for medium range impact, that is for $L^v_{0.1}$ and $D^v(1)$. It is seen that smaller g-values result in shorter range of impact and a more uniform flow field. The comparison shows that the length-measure and variation-measure defined in this work can improve the characterization of fabrics compared to the CFM-measure alone. Further, the new measures show additional features when characterizing fabrics, which has to be further understood. Some open questions remain. Why is the measured values higher compared to the cylinder study, and what effects are the reasons behind the discrepancies for $a = 0.2, 0.3$ and $y/d = 0.5, 0.25$ for the length- and variation-measure? The feature of non-uniform cylinder diameters has to be considered.

Moreover, the absolute values of the measures for the fabrics are compared. The results agree with the industrial applications of the fabrics. Also in this regard, the effect from different diameters of threads has to be further studied, since the simulations clearly demonstrate that for Fabric B, the large threads of the second layer lead to flow field patterns which could result in drainage marking. It is indicated that the wave-length of the flow periodicity is important as a fabric design parameter.

In this work, the flow over cylinders and fabrics is investigated, without the presence of any fibers. The results indicate what happens during the initial forming process, when the fabric structure governs the flow. Later during forming, when more fibers accumulate, the flow field will change. The effect of this change is a relevant topic for future research. As was seen for Fabric B (Figure 30), the larger threads in the second layer have a striking impact on the upstream flow. This could equally well be true for the flow in the later part of the lay down, that the fabric structure still have an important impact on the flow since the diameter of the threads are much larger compared to the thickness of the fibers. These effects could be studied in the two-dimensional setup by letting small cylinders flow down onto the fabric and investigate how the flow field changes, but also by positioning a large number of small cylinders on top of the larger cylinders investigating the resulting flow field.

Finally, the results in this paper show how the most elementary cylinder configurations affect the upstream flow features, information necessary to further understand the flow over industrial fabrics. The upstream flow measures defined in this work can be used to characterize forming fabrics, and the fundamental conclusions from the cylinder study hold true also for forming fabrics. The additional parameters of the forming fabric geometry, which are neglected in the cylinder study, seem to introduce additional features, which have to be studied further to clarify all aspects of the new measures. A natural next step would be to investigate how non-uniform cylinder diameters and non-uniform spacings in the two-row configurations affect the upstream flow. Thereafter, three-dimensional cylinder configurations would be useful to study. To further understand the paper formation, the interaction between fluid and fibers, and the later stage of the lay down, are important topics for future research. As is shown in this work, simulations of the flow over industrial forming fabrics are fully possible with the presented numerical method, with excellent agreement with experimental data. Therefore, simulations together with the proposed impact measures

enable characterization of fabrics that is not possible with experimental investigation alone.

Acknowledgments: This work is a part of the ISOP (Innovative Simulation of Paper) project which is performed by a consortium consisting of Albany International, Stora Enso and Fraunhofer-Chalmers Centre.

Conflict of interest: The authors declare no conflicts of interest.

References

Benard, H. (1908) Formation de centres de giration à l'arrière d'un obstacle en mouvement. C. R. Acad. Sci. 147:839–842.

Bird, B., Stewart, W., Lightfoot, E. Transport Phenomena. Wiley, New York, 2002.

Danby, R. (1986) The impact of multilayer fabrics on sheet formation and wire mark. Pulp Pap. Can. 87(8):69–74.

Doormaal, J.V., Raithby, G. (1984) Enhancements of the simple method for predicting incompressible fluid flows. Numer. Heat Transf.. 7(2):147–163.

Gilchrist, S., Green, S.I. (2009) Experimental investigation of flow through a bank of cylinders of varying geometry. J. Fluids Struct. 25(3):506–518.

Green, S.I., Wang, Z., Waung, T., Vakil, A. (2008) Simulation of the flow through woven fabrics. Comput. Fluids 37(9):1148–1156.

Helle, T. (1978) How forming fabric design affects drainage and release. Pulp Pap. Can. 79(11):91–98.

Huang, Z., Olson, J.A., Kerekes, R.J., Green, S.I. (2006) Numerical simulation of the flow around rows of cylinders. Comput. Fluids 35(5):485–491.

Von Karman, T., Rubach, H. (1912) Über den Mechanismus des Flüssigkeits- und Luftwiderstandes. Phys. Z. 13(2):49–59.

Kettil, G. (2016) A novel fiber interaction method for simulation of early paper forming. Licentiate thesis, Chalmers University of Technology, Gothenburg, Sweden.

Kortelainen, P., Kilpeläinen, R., Taipale, S., Marin, A., Metsäranta, S., Lohm, S., Sjöblom, E. (2008) Forming fabrics. In: Papermaking Part 1, Stock Preparation and Wet End, Ed. Paulapuro, H. Paperi ja Puu Oy, Helsinki. pp. 310–340.

Mark, A., Rundqvist, R., Edelvik, F. (2011a) Comparison between different immersed boundary conditions for simulation of complex fluid flows. Fluid Dyn. Mater. Proc.. 7(3):241–258.

Mark, A., Svenning, E., Rundqvist, R., Edelvik, F., Glatt, E., Rief, S., Wiegmann, A., Fredlund, M., Lai, R., Martinsson, L., Nyman, U. (2011b) Microstructure simulation of early paper forming using immersed boundary methods. Tappi J. 10(11):23–30.

Mark, A., van Wachem, B.G.M. (2008) Derivation and validation of a novel implicit second-order accurate immersed boundary method. J. Comput. Phys. 227(13):6660–6680.

Pozdziech, O., Grundmann, R. (2007) A systematic approach to the numerical calculation of fundamental quantities of the two-dimensional flow over a circular cylinder. J. Fluids Struct. 23(3):479–499.

Rhie, C., Chow, W. (1983) Numerical study of the turbulent flow past an airfoil with trailing edge separation. AIAA J. 21(11):1527–1532.

Roshko, A. (1954) On the development of turbulent wakes from vortex streets, NACA Report, Washington, D. C., USA, pp. 1–25.

Svenning, E., Mark, A., Edelvik, F., Glatt, E., Rief, S., Wiegmann, A., Martinsson, L., Lai, R., Fredlund, M., Nyman, U. (2012) Multiphase simulation of fiber suspension flows using immersed boundary methods. Nord. Pulp Pap. Res. J. 27(2):184–191.

Tritton, D.J. (1959) Experiments on the flow past a circular cylinder at low Reynolds numbers. J. Fluid Mech. 6(4):547–567.

Vakil, A., Olyaei, A., Green, S.I. (2009) Three-dimensional geometry and flow field modeling of forming fabrics. Nord. Pulp Pap. Res. J. 24(3):342–350.

Zdravkovich, M.M. (1977) Review – review of flow interference between two circular cylinders in various arrangements. J. Fluids Eng. 99(4):618–633.

Zdravkovich, M.M. Flow around circular cylinders. Vol. 1: Fundamentals. Oxford Univesity Press, Oxford, 1997. pp. 3–16.